ARTICLE

Ataxia-telangiectasia mutated interacts with Parkin and induces mitophagy independent of kinase activity. Evidence from mantle cell lymphoma

Aloke Sarkar,[1] Christine M. Stellrecht,[1,2] Hima V. Vangapandu,[1] Mary Ayres,[1] Benny A. Kaipparettu,[3] Jun Hyoung Park,[3] Kumudha Balakrishnan,[1,4] Jared K. Burks,[5] Tej K. Pandita,[6] Walter N. Hittelman,[1] Sattva S. Neelapu[4] and Varsha Gandhi[1,2,5]

[1]Department of Experimental Therapeutics, The University of Texas MD Anderson Cancer Center; [2]The University of Texas Graduate School of Biomedical Sciences at Houston; [3]Department of Molecular and Human Genetics, Dan L. Duncan Comprehensive Cancer Center, Baylor College of Medicine; [4]Department of Lymphoma/Myeloma, The University of Texas MD Anderson Cancer Center; [5]Department of Leukemia, The University of Texas MD Anderson Cancer Center and [6]Department of Radiation Oncology, The Houston Methodist Research Institute, Houston, TX, USA

Ferrata Storti Foundation

Haematologica 2021
Volume 106(2):495-512

ABSTRACT

Ataxia telangiectasia mutated (ATM), a critical DNA damage sensor with protein kinase activity, is frequently altered in human cancers including mantle cell lymphoma. Loss of ATM protein is linked to accumulation of nonfunctional mitochondria and defective mitophagy in both murine thymocytes and in ataxia-telangiectasia cells. However, the mechanistic role of ATM kinase in cancer cell mitophagy is unknown. Here, we provide evidence that FCCP-induced mitophagy in mantle cell lymphoma and other cancer cell lines is dependent on ATM but independent of its kinase function. While Granta-519 mantle cell lymphoma cells possess single copy kinase-dead ATM and are resistant to FCCP-induced mitophagy, both Jeko-1 and Mino cells are ATM-proficient and induce mitophagy. Stable knockdown of ATM in Jeko-1 and Mino cells conferred resistance to mitophagy and was associated with reduced ATP production, oxygen consumption, and increased mitochondrial reactive oxygen species. ATM interacts with the E3 ubiquitin ligase Parkin in a kinase-independent manner. Knockdown of ATM in HeLa cells resulted in proteasomal degradation of GFP-Parkin which was rescued by the proteasome inhibitor, MG132, suggesting that the ATM-Parkin interaction is important for Parkin stability. Neither loss of ATM kinase activity in primary B-cell lymphomas nor inhibition of ATM kinase in mantle cell lymphoma, ataxia-telangiectasia and HeLa cell lines mitigated FCCP- or CCCP-induced mitophagy suggesting that ATM kinase activity is dispensable for mitophagy. Malignant B-cell lymphomas without detectable ATM, Parkin, Pink1, and Parkin-Ub^{Ser65} phosphorylation were resistant to mitophagy, providing the first molecular evidence of the role of ATM in mitophagy in mantle cell lymphoma and other B-cell lymphomas.

Introduction

Mitochondria are indispensable for generating the solitary cellular energy currency, namely ATP, *via* oxidative phosphorylation and yet they exert damaging functions in altered pathophysiological scenarios including cancer.[1-5] Reactive oxygen species (ROS) emanating from mitochondria can cause inevitable damage to these organelles' own histone-devoid circular DNA with minimum proof-reading capacity encoding 37 genes - the prerequisite of the mitochondrial DNA (mtDNA) electron transport chain. Widespread metabolic reprogramming, excessive generation

Correspondence:
VARSHA GANDHI
vgandhi@mdanderson.org

Received: August 9, 2019.
Accepted: January 31, 2020.
Pre-published: February 6, 2020.

https://doi.org/10.3324/haematol.2019.234385

of ROS due to leakage of electrons from complexes I and III of the electron transport chain,[6] and dysregulation of fundamental cellular functions describe abnormal mitochondria that are structurally and functionally different from their normal counterparts.[7-9] Maintenance of mitochondrial homeostasis in a cell is dependent on strict and highly dynamic mitochondrial fusion and fission cycles[10,11] guided by two opposing events: reparation of damage by fusion and removal of damage by fission. In a unique scenario, a defective mitochondrion incapable of making ATP *via* F_1-F_0-ATPase, instead produces excessive amounts of ROS and is forced to consume ATP to generate membrane potential ($\Delta\Psi_m$), impeding normal metabolic function.[12] Although low levels of mitochondrial damage can be repaired by complementation through the fusion process, an excessively damaged pool of mitochondria may endanger functional mitochondria during their coexistence, affecting the quality control of mitochondria.[12,13] Cells have an inherent capacity to sense damaged mitochondria and selectively degrade these defective organelles by a process called mitochondrial autophagy or mitophagy.

During mitophagy, Pink1 accumulates on the outer membrane of depolarized mitochondria[14] and recruits the cytosolic ubiquitin ligase Parkin and phosphorylates both Parkin and ubiquitin, resulting in Parkin activation. Activated Parkin in turn ubiquitylates scores of outer mitochondrial membrane proteins of depolarized mitochondria followed by recruitment of multiple autophagy cargo adaptors, such as OPTN and NDP52. Finally all these cargos bind directly to LC3 in the autophagosome leading to degradation of the entire mitochondrion within autophagolysosomes.[15]

Ataxia telangiectasia mutated (ATM) is obligatory to initiate cellular responses to DNA double-strand breaks and DNA repair to preserve genomic integrity, and loss of ATM results in genetic disorders characterized by neurodegeneration, immunodeficiency, and cancer.[16-20] ATM also possesses non-nuclear functions associated with its cytoplasmic localization in various cell types[21,22] and loss of ATM leads to increased accumulation of ROS and aberrant mitochondria leading to abnormal mitochondrial homeostasis and may trigger cancer progression.[16,23] Further, loss of ATM leads to global dysregulation of ribonucleotide reductase activity and abrogation of mitochondrial biogenesis and mtDNA content.[24] Cells from patients with ataxia telangiectasia (A-T) contain a greater mitochondrial mass and are defective in mitochondrial respiration compared to wild-type (WT) fibroblasts.[25] However, none of the phenotypic abnormalities commonly observed in ATM-deficient cells are explained by defects in canonical DNA damage response pathways, particularly in neurodegeneration, cancer predisposition, and premature aging.

Even though ATM is frequently mutated in cancer, a comprehensive study relating ATM dysfunction in mitophagy in cancer cells and in cancer patients is lacking. Mantle cell lymphoma (MCL) is a genetically unstable and fatal B-cell non-Hodgkin lymphoma, in which deletions or inactivating mutations in the *ATM* gene are frequently acquired (40-75% of cases).[26,27] We demonstrate the role of ATM in mitophagy using MCL cell lines and primary cells obtained directly from patients, and show that ATM controls mitophagy through interaction with Parkin in a kinase-independent manner.

Methods

Cell lines and primary lymphoma analysis

Cell lines are described in the *Online Supplementary Methods*. Primary B-cell lymphomas were obtained following informed consent from every patient on an Institutional Review Board-approved protocol and were in accordance to the declaration of Helsinki.

Reagents and antibodies

The reagents and antibodies used in this study are presented in *Online Supplementary Table S1*.

Ionizing radiation, intracellular staining and flow cytometry analysis

Ionizing radiation (IR) or neocarzinostatin was used to induce DNA damage. Two potent uncoupling agents, CCCP or FCCP, were used to induce mitophagy. Cells were stained with appropriate dyes to determine mitophagy, total and mitochrondrial ROS (mROS) and acquired by flow cytometry (FCS) assay.

Plasmids, lentiviral infection and transfection

pcDNA3.1$^+$ Flag-His-ATM wt (#31985) and pcDNA3.1$^+$ Flag-His-ATM kd (#31986) were obtained from Addgene. GFP-Parkin, GFP-LC3 and GFP vector plasmids were gifts. Cells were transfected with Lipofectamine 2000 (Invitrogen) or Fugene6 (Promega). Lentiviral non-target short hairpin (sh)RNA and Mission shATM clones and lentivirus particles were prepared according to the manufacturer's instructions (Sigma).

Immunoprecipitation and co-immunoprecipitation experiments

Standard immunoprecipitation and co-immunoprecipitation experiments were performed by transfecting plasmids in either HEK293T, WT-HeLa or A-T cells.

Measurement of nucleoside triphosphates

Intracellular nucleotides were determined by high performance liquid chromatography analysis after perchloric acid extraction.

Oxygen consumption analyses

Cellular oxygen consumption rate was measured by a standard Seahorse assay (Seahorse Bioscience, Billerica, MA, USA).

Cell fractionation and immunoblot analysis

Cell fractionation was performed using either a NE-PER kit (Thermo Fisher) or Cell fractionation kit (Abcam; AB109719) following the manufacturers' guidelines. Protein lysates and immunoblots were prepared and protein bands were quantified using a LI-COR Odyssey CLx Infrared Imaging System.

Quantitative reverse-transcriptase polymerase chain reaction and mitochondrial DNA analysis

Total RNA was isolated using an RNeasy Mini Kit and the reverse transcriptase reaction was performed using a RevertAid™ H Minus First Strand cDNA Synthesis kit. Reverse transcriptase polymerase chain reaction (RT-PCR) was performed using the SYBR® Green PCR Master Mix. mtDNA copy number was analyzed in total DNA by quantitative PCR (qPCR) using mtDNA- and nuclear DNA-specific primers (PMC3769921) and the copy number was calculated as described before.[28]

Confocal analysis

Cells were grown in chamber slides, stained with primary antibodies and processed for standard fixation for confocal analysis using an Olympus FV1000 laser confocal microscope with a 40x 1.3-oil immersion lens. All captured images were analyzed using 3I Slidebook 5.5 (SB645.0.0.30) software.

Statistical analysis

All numerical results are presented as mean ± standard error of mean. The statistical significance of differences was analyzed using a Student *t*-test (paired) or analysis of variance. The statistical computations were conducted with Prism (GraphPad Software, San Diego, CA, USA).

Full details of the methods are available in the *Online Supplementary Methods* file.

Results

ATM-proficient and -deficient mantle cell lymphoma cell lines display differential sensitivity to FCCP-induced mitophagy.

To determine the role of ATM in mitophagy we used three MCL cell lines (Granta-519, Jeko-1 and Mino). The ATM-deficient Granta-519 line possesses a single copy of the *ATM* gene harboring a point mutation within the conserved residues of the kinase domain while both Jeko-1 and Mino cells are ATM-proficient.[29,30] These cell lines contain the distinguishing t(11;14)(q13;q32) translocation resulting in cyclin D1 (CCND1) overexpression.[31] Cells were treated with the mitochondrial uncoupler FCCP to induce mitophagy. Induction of mitophagy was associated with loss of mitochondrial membrane potential ($\Delta\Psi_m$) in both Jeko-1 and Mino cells, while Granta-519 retained intermediate to high $\Delta\Psi_m$ and greater mitochondrial mass (Figure 1A, B). Both basal mROS and global ROS were relatively higher in Granta-519 (Figure 1C-E) compared to other MCL cell lines. Typically mitophagy is accompanied by loss of both COXIV and the mitochondrial outer membrane protein Tom20. Immunoblot analysis revealed defective FCCP-induced mitophagy in Granta-519 as COXIV and Tom20 levels were not affected by FCCP treatment while they were reduced in FCCP-treated Jeko-1 and Mino cells (Figure 1F) with <10% cell death *(Online Supplementary Figure S1A)*. Phosphorylation of ATM^{Ser1981} or ATM targets, Kap1^{Ser824} and Smc1^{Ser966} was detected in both Jeko-1 and Mino cells but not in Granta-519 (Figure 1F). FCS analysis also confirmed IR-induced ATM^{Ser1981} and

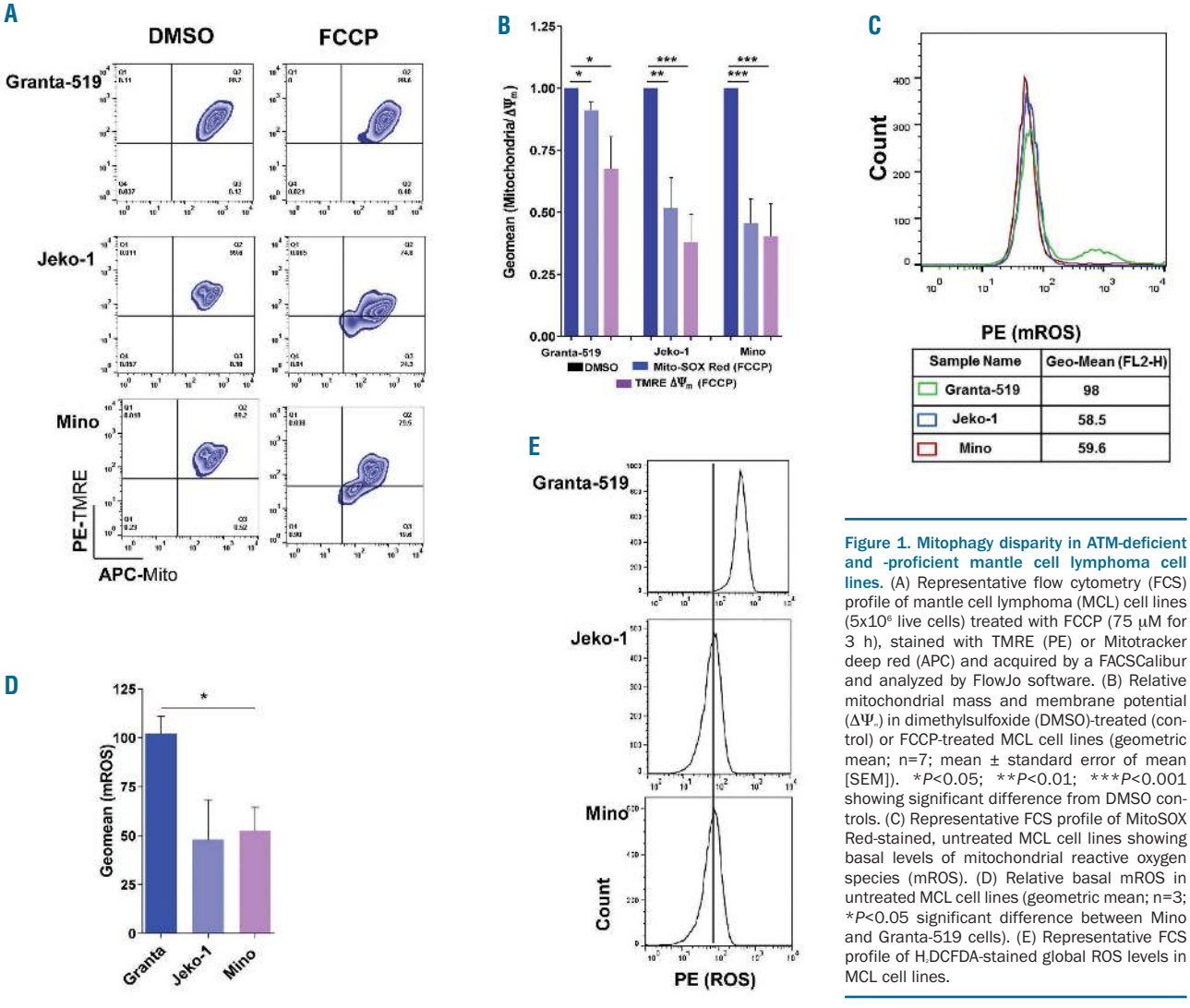

Figure 1. Mitophagy disparity in ATM-deficient and -proficient mantle cell lymphoma cell lines. (A) Representative flow cytometry (FCS) profile of mantle cell lymphoma (MCL) cell lines ($5x10^6$ live cells) treated with FCCP (75 μM for 3 h), stained with TMRE (PE) or Mitotracker deep red (APC) and acquired by a FACSCalibur and analyzed by FlowJo software. (B) Relative mitochondrial mass and membrane potential ($\Delta\Psi_m$) in dimethylsulfoxide (DMSO)-treated (control) or FCCP-treated MCL cell lines (geometric mean; n=7; mean ± standard error of mean [SEM]). *P<0.05; **P<0.01; ***P<0.001 showing significant difference from DMSO controls. (C) Representative FCS profile of MitoSOX Red-stained, untreated MCL cell lines showing basal levels of mitochondrial reactive oxygen species (mROS). (D) Relative basal mROS in untreated MCL cell lines (geometric mean; n=3; *P<0.05 significant difference between Mino and Granta-519 cells). (E) Representative FCS profile of H_2DCFDA-stained global ROS levels in MCL cell lines.

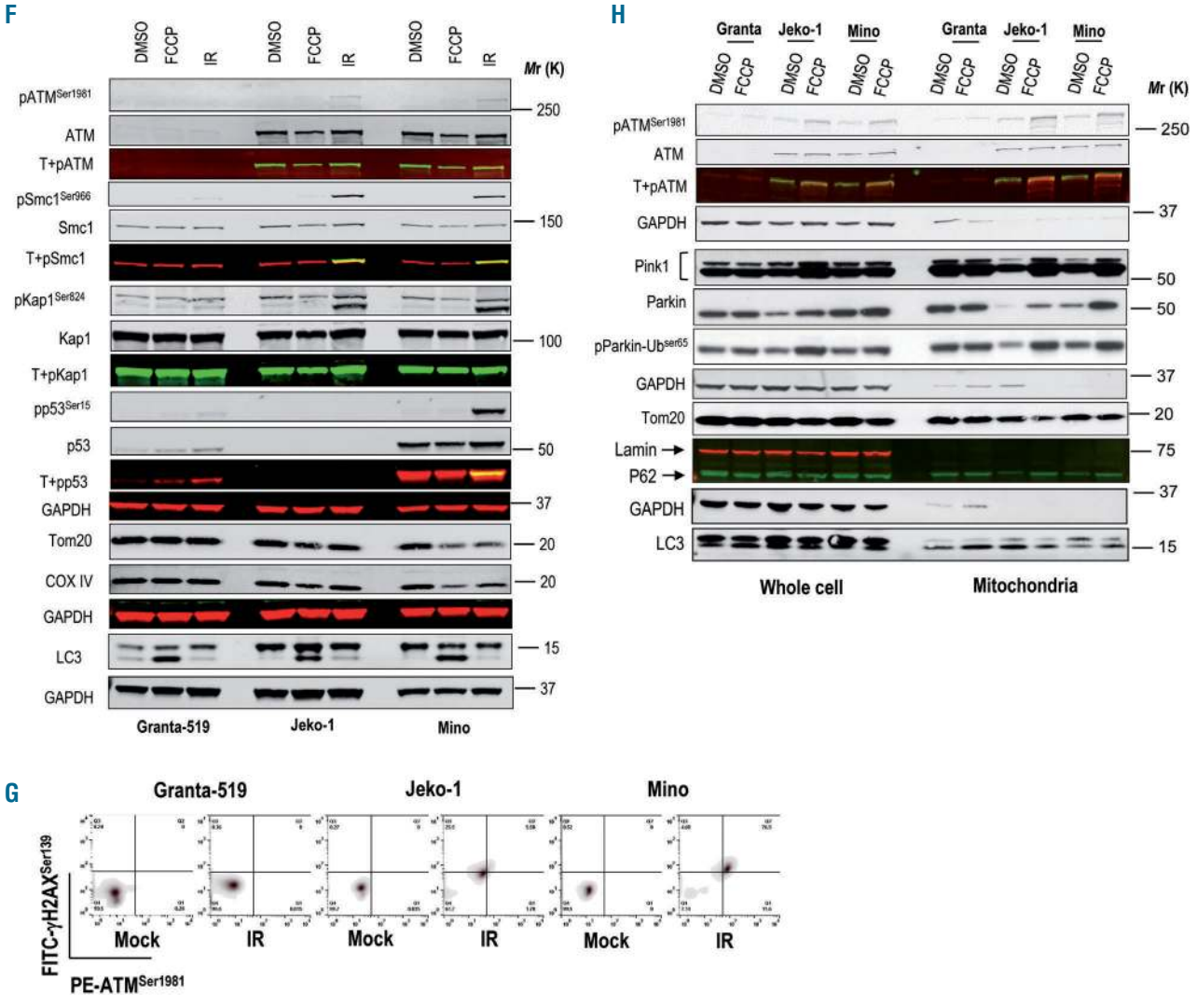

Figure 1. (Continued from the previous page) (F) Immunoblot analysis of MCL cells lines (30 μg total protein) treated with DMSO or FCCP, as in (A) or irradiation (IR) ($5x10^6$ cells; 5 Gray) showing disparities in mitophagy. Separate blots were cut into pieces and probed with the indicated antibodies. Total and phosphorylated bands were merged and shown in color for specificity. Phospho-ATM, Smc-1, Kap-1 and p53 proteins represent DNA damage sensors. Decreases in Tom20 and COXIV levels reflect mitophagy and LC3 lipidation represents global autophagy. GAPDH was probed as a loading control each time. (G) FCS analysis showing IR (5 Gray)-induced $ATM^{Ser1981}$ and $H2AX^{Ser139}$ phosphorylation in MCL cell lines. One hour after IR treatment, cells were washed and stained with PE-$ATM^{Ser1981}$ and FITC-$H2AX^{Ser139}$, washed and acquired by a FACSCalibur and analyzed by FlowJo software, as in (1A). (H) Cell fractionation immunoblot analysis of MCL cell lines ($30x10^6$ cells per treatment) showing basal and FCCP (75 μM for 3 h)-induced mitophagy from whole cells (20 μg) and mitochondrial fractions (10 μg). GAPDH was probed to distinguish whole cell and mitochondrial proteins. Nuclear contamination in the mitochondrial fraction was detected by Lamin. Separate sets of blots were probed with the indicated antibodies. Parkin, phospho-Parkin and Pink1 were probed using an electrochemoluminescence method. Total and phosphorylated bands were merged and shown in color for specificity. GAPDH was probed as a loading control each time.

γH2AX^{Ser139} phosphorylations in both Jeko-1 and Mino cells but not in Granta-519 (Figure 1G). In contrast, global autophagy induced by FCCP, as detected by LC3 lipidation, was similar in all three cell lines indicating that ATM is not required for global autophagy. Furthermore, mitophagy was not affected by the loss of p53 in Jeko-1 cells demonstrating that p53 is not required for mitophagy.

Similar experiments on human A-T isogenic cell lines revealed ATM dependency of mitophagy, as reported earlier.[23] Further analyses confirmed that while autophagy was induced by CCCP in either cell line, mitophagy was restricted to only WT cells. Furthermore, we showed that A-T cells possess relatively lower levels of Pink1 and Parkin proteins with a significantly higher basal mROS level compared with the levels in WT cells (*Online Supplementary Figure S1B-F*).

Cell fractionation analysis revealed the presence of ATM and phospho-$ATM^{Ser1981}$ in the mitochondrial fraction of both Jeko-1 and Mino cells (Figure 1H). Although the majority of ATM protein was nuclear, some ATM was also detected in the cytoplasm of these cells (*Online Supplementary Figure S2A*). Mitophagy was detected in both Jeko-1 and Mino cells, but not in Granta-519, as evidenced by the loss of Tom20, and was associated with both Parkin and phospho-Parkin-UB^{Ser65} activation (Figure 1H and *Online Supplementary Figure S2B*). Interestingly, despite selective induction of mitophagy in both Jeko-1 and Mino cells, neither p62 recruitment nor autophagy (LC3 lipidation) was affected in ATM-deficient Granta-519 cells. Together, these data suggest that a specific defect in mitophagy, but not in global

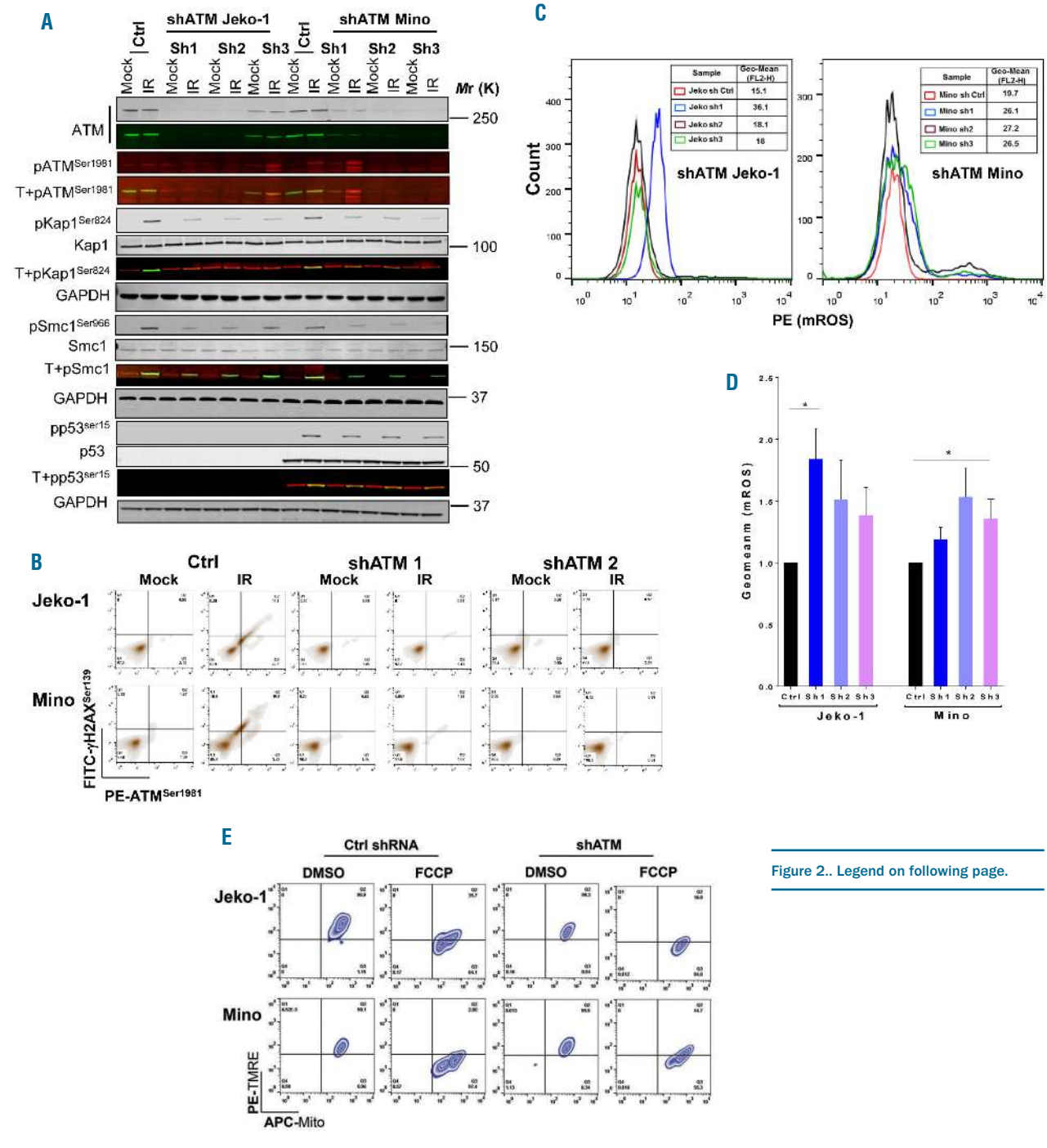

Figure 2.. Legend on following page.

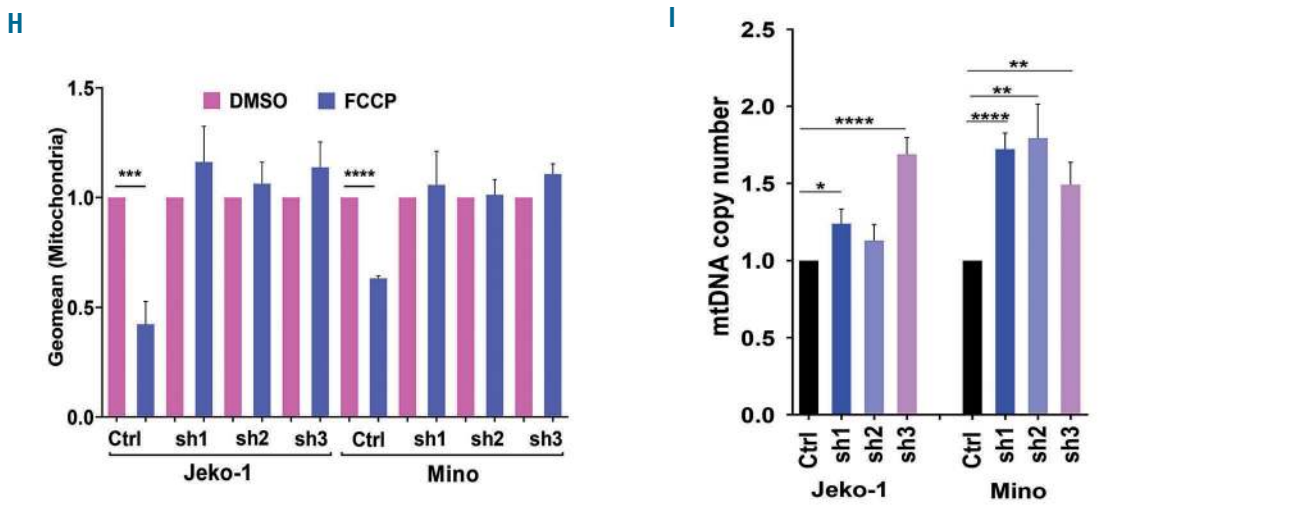

Figure 2. Defective mitophagy in mantle cell lymphoma shATM cell lines. (A) Immunoblot analysis of stable lentiviral knockdown of ATM in Jeko-1 and Mino cells showing irradiation (IR)-induced defective phospho-ATM^{Ser1981}, -Kap1^{Ser824}, -Smc1^{Ser966} and -p53^{Ser15} expression. Separate blots (20 μg total protein) were cut into pieces and probed with the indicated antibodies. Total and phosphorylated bands were merged and are shown in color for specificity. GAPDH was probed as a loading control each time. (B) Representative flow cytometry (FCS) profile showing IR (as in Figure 1G)-induced ATM^{Ser1981} and H2AX^{Ser139} phosphorylation in control and shATM mantle cell lymphoma (MCL) cell lines. (C) Representative FCS profile of MitoSOX Red-stained cells showing basal levels of mitochondrial reactive oxygen species (mROS) in control and shATM MCL cell lines. (D) Relative geometric mean of mROS levels in basal and untreated (as in Figure 1F) MCL shATM clones (n=3; mean ± standard error of mean [SEM]; *P<0.05) showing significant difference from respective control shRNA. (E) Representative FCS profile (as in Figure 1A) showing mitochondrial mass and mitochondrial membrane potential ($\Delta\Psi_m$) in control or shATM clones treated with dimethylsulfoxide (DMSO) or FCCP in MCL cell lines. (F) Immunoblot analysis of whole cell extracts (30 μg total protein) from Jeko-1 and Mino shATM clones treated with FCCP or DMSO. Separate blots were cut into pieces and probed with the indicated antibodies. GAPDH was probed as a loading control each time. (G) Tom20 densitometry analysis from triplicate experiments (Figure 2F) with data presented as mean ± SEM; *P<0.05, **P<0.01: significant differences from respective DMSO controls. (H) Relative geometric mean of mitochondrial mass in DMSO- or FCCP-treated (as in Figure 1B) MCL control and shATM clones (n=4; mean ± SEM). ***P<0.001, ****P<0.0001: significant differences from respective DMSO controls. (I) Quantitative polymerase chain reaction analysis of mitochondrial DNA copy number in untreated shRNA control and shATM MCL clones showing mean ± SEM (=3). *P<0.05, **P<0.001, ****P<0.0001: significant differences from respective control shRNA. mtDNA: mitochondrial DNA.

autophagy resulted from the loss of functional ATM in Granta-519 cells.

Stable knockdown of ATM elicits high mitochondrial DNA copy number and defective mitophagy in mantle cell lymphoma cell lines

To further delineate the role of ATM in mitophagy, we stably knocked down ATM in Jeko-1 and Mino cells *via* lentiviral shATM transduction. Immunoblot analysis confirmed loss of ATM protein in the shATM clones compared to control shRNA and were also defective in IR-induced ATM^{Ser1981}, Kap1^{Ser824}, Smc1^{Ser966} and p53^{Ser15} phosphorylation as well as IR-induced ATM^{Ser1981} and γH2AX^{Ser139} phosphorylation, as shown by FCS analysis (Figure 2A, B).

These shATM clones were also found to produce relatively higher mROS (Figure 2C, D), defective in FCCP-induced mitophagy and retained higher mitochondrial VDAC1, Tom20, COXIV and mtDNA copy number as compared to control shRNA. Neither, autophagy (LC3 lipidation) nor FCCP-induced loss of $\Delta\Psi_m$ was affected by ATM ablation (Figure 2E-I and *Online Supplementary Figure S3A-C*). Therefore, loss of ATM provokes accumulation of mROS, preservation of mitochondrial mass, and inhibition of mitophagy in human cancer cells.

Loss of ATM is associated with less mitochondrial ATP generation

Endogenous levels of ATP and UTP were significantly higher in Jeko-1 and Mino cells (*Online Supplementary Figure S4A*) than in Granta-519, indicating higher respiratory capacity. Further, ATM ablation in MCL cell lines resulted in significantly less ATP production (Figure 3A). This decline in ATP-linked respiration in the shATM clones resulted in depletion in the ATP pool, basal oxygen consumption rate (OCR) or in their respective stress-induced spare respiratory capacities (SRC) (Figure 3B-D). The maximal ATP output of mitochondria can be determined by addition of the mitochondrial uncoupler, FCCP, which collapses the proton gradient and generates $\Delta\Psi_m$ and triggers maximal OCR and substrate oxidation by complex IV. Moreover, SRC allows us to determine the ability of the cells to respond to increased energy demands following FCCP treatment. Thus, the observed decreases in both basal OCR and SRC in shATM clones were consistent with significant reductions in the intracellular ATP pool in ATM-depleted cells. Consistent with these findings, we found higher OCR and SRC in WT cells than in A-T cells (*Online Supplementary Figure S4B,C*).

ATM interacts with and confers Parkin stability in a kinase-independent manner

Having observed that ATM ablation impedes mitophagy prompted us to determine the role of ATM kinase in Parkin-mediated mitophagy in HeLa cells. ATM in WT HeLa cells was stably knocked down (Kd-ATM HeLa) by lentiviral shATM infection (Figure 4A). The distributions of global, nuclear, cytoplasmic, and mitochondrial ATM foci were quantified by confocal analysis using a cellular masking method (*Online Supplementary Figure S5A*). As expected, significantly more abundant ATM foci were observed in all three compartments in WT cells than in Kd-ATM cells (Figure 4B-D). CCCP treatment resulted in greater mitochondrial ATM-Tom20 co-localization than in control cells treated with dimethylsulfoxide. While both global and cytoplasmic ATM foci remained

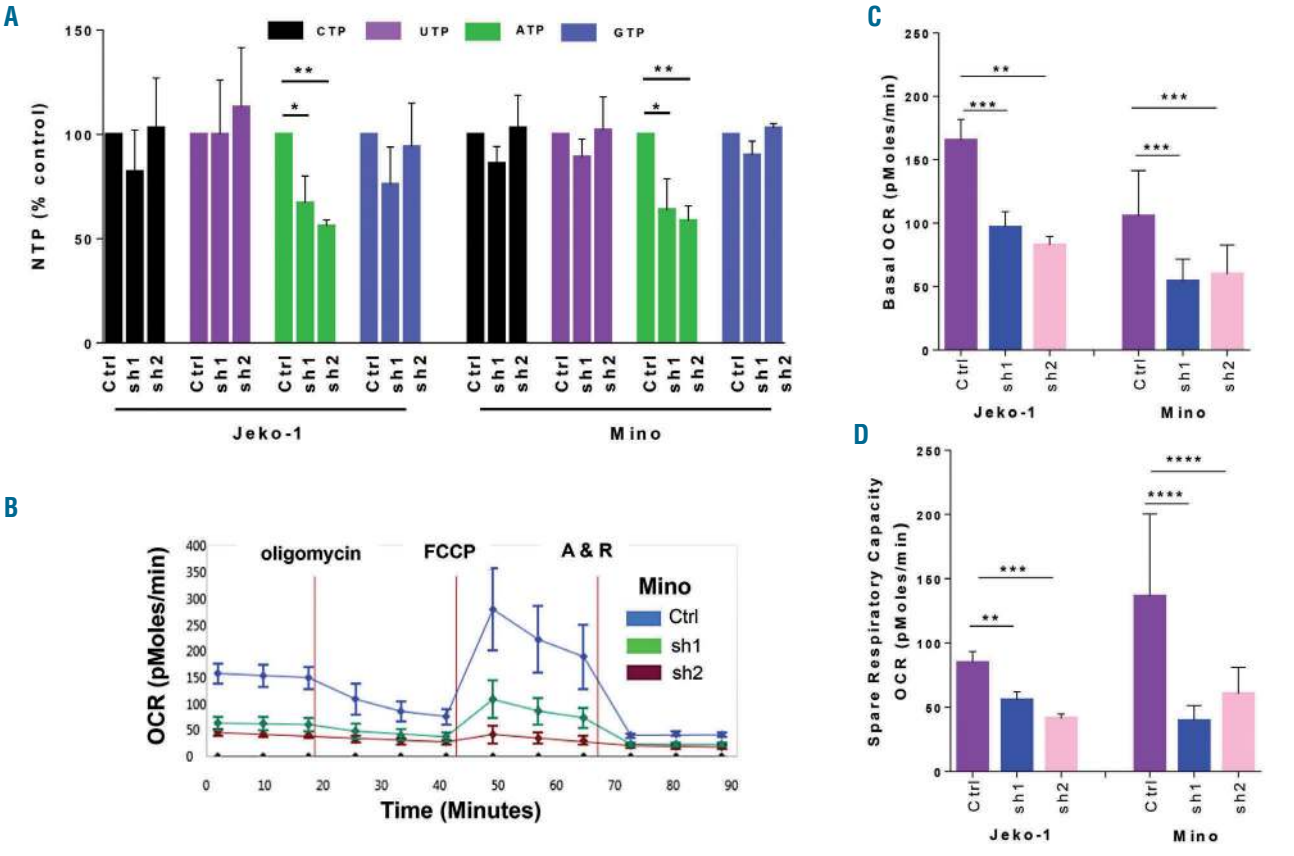

Figure 3. Decreased mitochondrial respiration in shATM mantle cell lymphoma cell lines. (A) High performance liquid chromatography analysis of basal intracellular nucleotide (NTP) levels in untreated mantle cell lymphoma (MCL) control and shATM clones showing mean ± standard error of mean (SEM) (n=3). *P<0.05, **P<0.01: significant differences from respective control shRNA. (B) Graphical representation of the mitochondrial stress test assay in untreated Mino control and shATM clones (8×10^4 live cells). Treatment with a mitochondrial ATP synthesis uncoupler, FCCP, resulted in the maximal oxygen consumption rate (OCR) by the respiratory chain. Furthermore, addition of rotenone and antimycin A (complex I and III inhibitors, respectively) prevented the transfer of electrons and thereby diminished OCR, indicating an overall reduction in mitochondria-linked aerobic respiration and ATP production in shATM cells. (C) Relative OCR in untreated MCL shATM clones showing mean ± SEM; (n=3). **P<0.01, ***P<0.001: significant differences from control shRNA. (D) Relative mitochondrial spare respiratory capacity in untreated MCL shATM clones showing mean ± SEM; (n=3). **P<0.01, ***P<0.001, ****P<0.0001: significant differences from control shRNA.

unchanged following CCCP treatment, the loss of nuclear ATM and significant gain in mitochondrial ATM likely reflects translocation of ATM from the nucleus to the mitochondria.

Confocal analysis also showed significantly higher mass of mitochondrial nucleoids in Kd-ATM HeLa cells than in WT controls (Figure 4E,F). Since HeLa cells lack detectable Parkin expression,[32] both WT and Kd-ATM HeLa cells were transfected with GFP-Parkin plasmid to generate stable HeLa GFP-Parkin isogenic cell lines proficient or deficient in ATM. Surprisingly, while transient GFP-Parkin expression was fairly equal in both WT and Kd-ATM cell lines (Figure 4G), we failed to generate stable GFP-Parkin-expressing Kd-ATM HeLa cells. However, neither stable expression of GFP-vector nor GFP-LC3 was affected, suggesting a specific defect in GFP-Parkin stability in Kd-ATM HeLa cells (Figure 4H). Cell fractionation studies following exposure to CCCP (Figure 4I) revealed the presence of ATM protein in both nuclear and mitochondrial fractions in WT but not in Kd-ATM cells. GFP-Parkin expression was detected in both cytoplasm and mitochondrial fractions, and CCCP treatment enriched the abundance of mitochondrial GFP-Parkin accumulation in WT cells, resulting in a decrease in Tom20 expression *via* mitophagy. In contrast, mitochondrial GFP-Parkin translocation was undetectable in Kd-ATM cells following CCCP treatment. However, the cellular distribution of the endogenous autophagy adaptor protein, p62/SQSTM1, was not affected in either of these cells, suggesting that autophagy is unrelated to the loss of ATM in HeLa cells. Confocal analysis reconfirmed that CCCP significantly induced mitochondrial GFP-Tom20 double-positive foci in WT cells compared to Kd-ATM cells (Figure 4J-L). We also showed that endogenous Parkin expression is significantly lower in the majority of the early passage MCL shATM cell lines than in control shRNA-transduced cells (Figure 4M, N). These data support the notion that defective mitophagy in MCL and HeLa shATM cells is likely due to lack of Parkin stability and mitochondrial Parkin translocation.

Parkin is known to autoubiquitinate at the UBL domain and undergo proteasomal degradation in the cytosol.[33] while endogenous Pink1 is known to be rapidly degraded by UBR1, UBR2 and UBR4 through the "N-end rule pathway".[34] Interestingly, the proteasome inhibitor, MG132 rescued loss of GFP-Parkin stability in Kd-ATM HeLa cells (Figure 5A upper panel; *Online Supplementary Figure S5B*). Surprisingly, endogenous Pink1 expression was lower in Kd-ATM cells than in WT ones and MG132 prevented Pink1 degradation in both cell lines (Figure 5A lower panel). The kinetics of GFP-Parkin degradation following cycloheximide treatment (Figure 5B, C) suggested a signif-

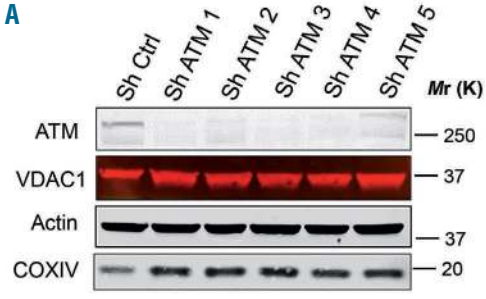

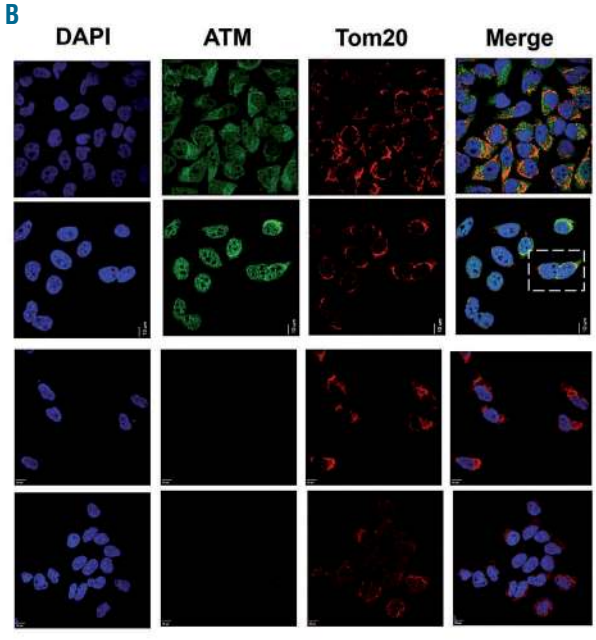

Figure 4. ATM is localized inside mitochondria: evidence from HeLa cells. (A) Immunoblot analysis (30 μg total protein) of five different stable lentiviral shATM in HeLa cells. A single blot was cut into pieces and probed with the indicated antibodies. Actin was probed as a loading control. (B) Representative confocal z-plane image analysis (scale: 10 μm) showing nuclear and extra-nuclear ATM localization in WT and Kd control (dimethylsulfoxide, DMSO) or CCCP-treated (50 μM for 3 h) HeLa cells. Nuclei are stained with DAPI. (C) Arrows in the inset of Figure 4B showing the localization of ATM in the nucleus (N), cytosol (C, green dots) or mitochondria (M, co-localized with Tom20, yellow dots). A Laplacian filter was used to identify both ATM and Tom20 co-localization in the merged image. (D) There were significantly fewer cellular ATM dots in whole cells and in all cellular compartments in Kd ATM compared to WT control cells. Significantly more mitochondrial ATM (co-localized ATM-Tom20 dots) was observed in WT HeLa cells treated with CCCP. WT control (162 cells), WT-CCCP (176 cells); Kd control (112 cells) and Kd-CCCP (121 cells) were scanned. Data represent mean ± standard error of mean (n=3 from separate passages of cell lines following GFP-Parkin transfection). *P<0.05, ****P<0.0001 significant differences from respective controls, as indicated. DAPI represents nuclear staining. (E). Representative confocal z-plane image of WT and Kd HeLa cells showing mitochondrial nucleoids. Untreated cells were stained with anti-DNA (red) antibody (scale: 10 μm). DAPI represents nuclear staining. (F) Significantly higher (****P<0.0001) mitochondrial nucleoids in untreated Kd compared to WT HeLa cells. WT (228 cells), and Kd (385 cells) were scanned from three separate passages of cell lines and plotted. (G) WT and Kd HeLa cells were transiently transfected with plasmids (3 μg of each pcDNA control or GFP-Parkin). Representative FCS profile showing GFP expression 36 h after transfection (left panel) or merged GFP subsets (right panel).

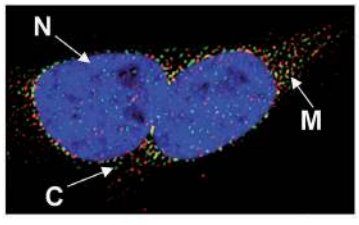

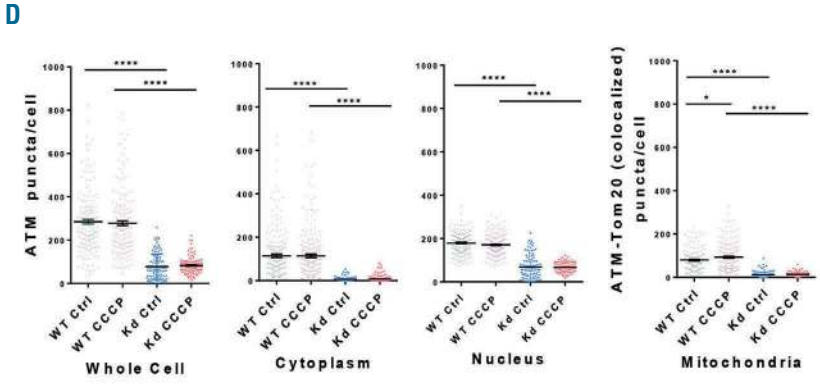

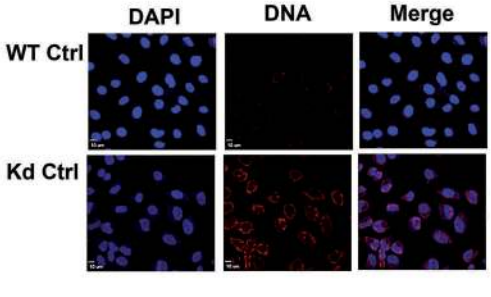

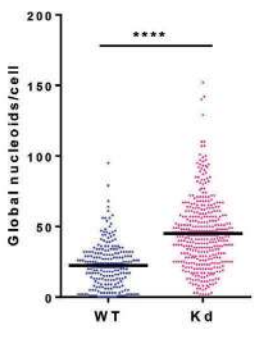

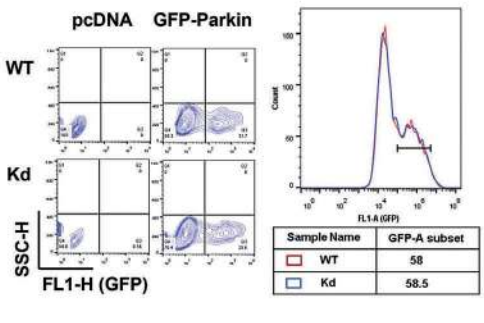

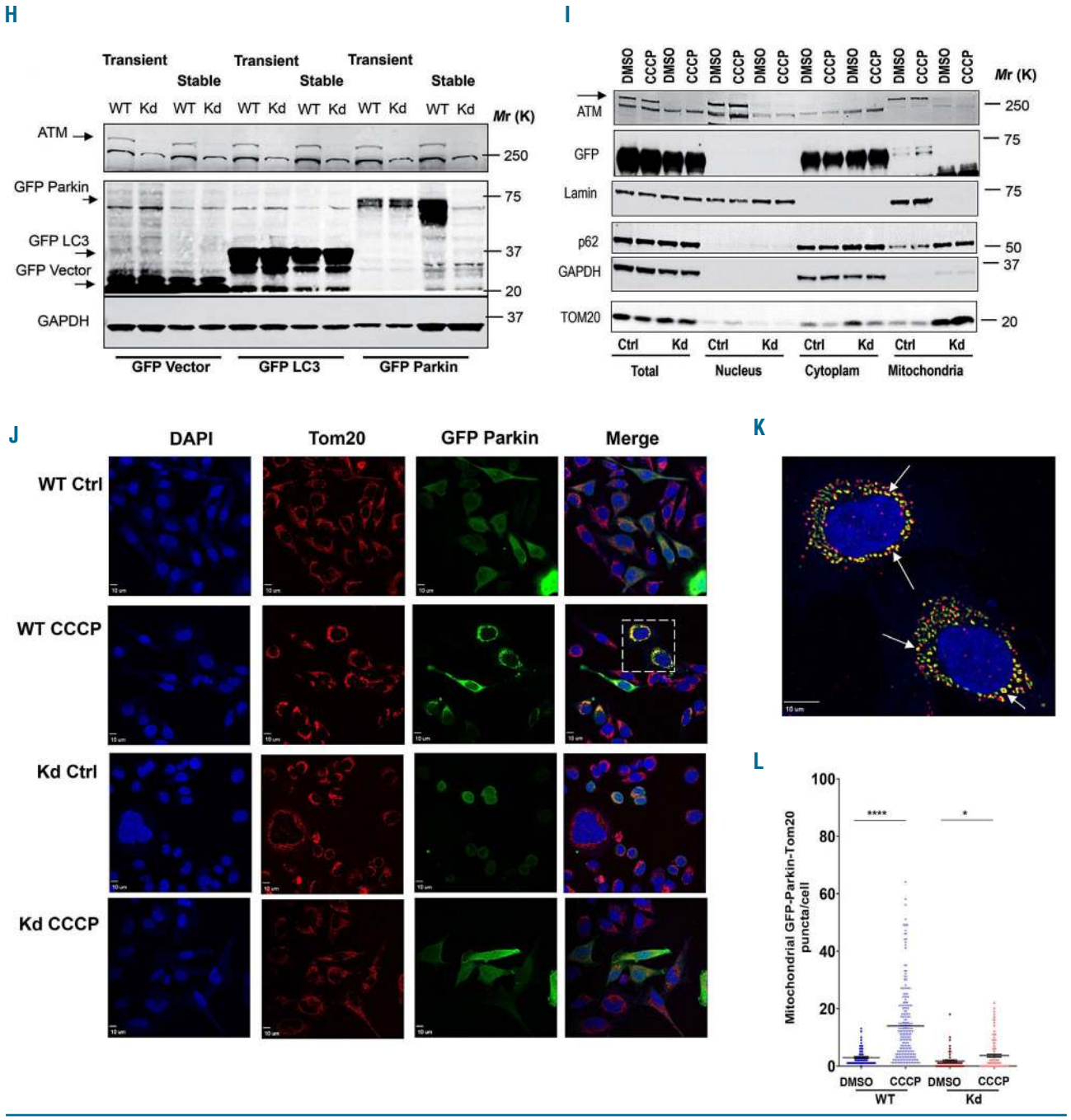

Figure 4. (Continued from the previous page). (H) Immunoblot analysis (30 μg total protein) showing ATM and GFP expression from transient (48 h) and stable (3 weeks) transfection with GFP vector, GFP-LC3 or GFP-Parkin plasmids in WT and Kd HeLa cells. A single blot was cut into pieces and probed with the indicated antibodies. GAPDH was probed as a loading control. (I) Cell fractionation immunoblot analysis of WT and Kd HeLa cells showing cellular GFP distribution following transient transfection with GFP-Parkin (48 h). Cells ($10x10^6$) treated with DMSO or CCCP (50 μM for 3 h) were fractionated and then 30 μg total or 10 μg each of nuclear, cytoplasmic, and mitochondrial proteins were loaded and probed with the indicated antibodies. Lamin and GAPDH were probed as nuclear and cytoplasmic loading controls. (J) Representative confocal z-plane image analysis (scale: 10 μm) 48 h after GFP-Parkin transfection, showing GFP-Parkin co-localization with the mitochondrial marker Tom20 in WT and Kd HeLa cells treated with DMSO (Ctrl) or CCCP (50 μM for 3 h). Nuclei were stained with DAPI. (K) Inset of Figure 4J, with arrows showing co-localization of GFP-Tom20 (yellow dots) inside mitochondria after WT HeLa cells had been treated with CCCP. A Laplacian filter was used to identify both GFP-Parkin and Tom20 foci revealing co-localization in the merged image. (L) CCCP treatment resulted in a greater abundance of mitochondrial GFP-Parkin-Tom20 co-localization in WT (****P<0.0001) compared to Kd (*P<0.05) HeLa cells. WT control (68 cells), WT-CCCP (200 cells); Kd control (59 cells) and Kd-CCCP (133 cells) were scanned from three separate passages of cell lines and plotted. (Continued on the next page)

icantly enhanced degradation of GFP in Kd-ATM cells than in WT HeLa cells. However, loss of ATM did not affect the stability or degradation of the long half-life (HSP90) or short half-life (MCl-1)[35] proteins. Real-time RT-PCR analysis from identical cells did not reveal any significant change in GFP expression (Figure 5D), arguing for a specific defect in GFP-Parkin protein stability in Kd-ATM HeLa cells.

This observation prompted us to investigate the role of ATM kinase activity in the ATM-Parkin interaction. GFP-Parkin-transfected WT Hela cells were immunoprecipitated with anti-ATM antibody (Figure 5E, F; *Online*

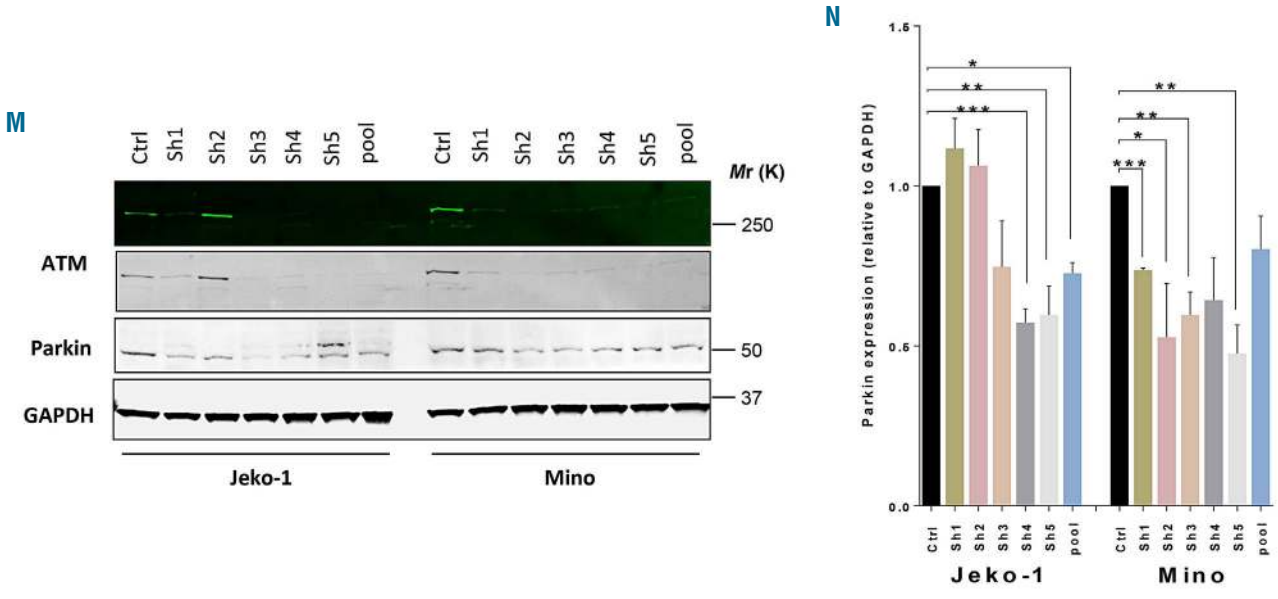

Figure 4. (Continued from the previous page). (M) Immunoblot analysis (30 µg total protein) from mantle cell lymphoma (MCL) shATM cell lines (between passage 2-5) showing loss of endogenous Parkin (electrochemoluminescence blot). Blots were cut into pieces and probed with the indicated antibodies. GAPDH was probed as a loading control. (N) Densitometry analysis showing basal Parkin expression from three separate replicates of MCL control and shATM clones. Data represent mean ± standard error of mean (n=3 from separate passages of cell lines until passage 5), *P<0.05, **P<0.01, ****P<0.0001: significant differences from respective controls, as indicated.

Supplementary Figure S6A). We showed that neither ATM kinase inhibitor (KU60019) nor neocarzinostatin treatment influenced their interaction, confirming that the ATM-Parkin interaction is kinase-independent. Similarly, the endogenous interaction of ATM-Parkin in the Mino cell line was also independent of ATM kinase inhibition and KU60019 did not inhibit the interaction when cells were treated with this in combination with FCCP (Figure 5G, H; *Online Supplementary Figure S6B*). The efficacy of KU60019 was demonstrated by loss of ATM^{Ser1981} and Kap1^{Ser824} phosphorylation (Figure 6D). In other experiments, A-T cells were co-transfected with either WT or kinase-dead (KD)-Flag-ATM and GFP-Parkin plasmids and immunoprecipitated with anti-Flag antibody. Analysis of the immunoprecipitates showed that both WT and Kd-ATM interacts with GFP-Parkin (*Online Supplementary Figure S6C,D*). Further immunoprecipitation analysis with anti-Parkin antibody from purified cytosolic and mitochondrial fractions from Mino cells suggests that the ATM-Parkin interaction was restricted in both these fractions (Figure 5I, J). In contrast, trypsin digestion of the mitochondrial fraction, which removes proteins from the outer membrane, revealed the presence of Parkin but not ATM in the inner membrane along with TIM23,[36] a specific inner membrane translocase. These data confirm that the ATM-Parkin interaction is restricted to the outer mitochondrial membrane.

ATM kinase is dispensable in mitophagy: evidence from mantle cell lymphoma, HeLa cells and primary B-cell lymphomas

The observed kinase-independent interaction of ATM-Parkin led us to test the role of ATM kinase function in mitophagy using pharmacological ATM inhibitors or activators. The ATM kinase inhibitor, KU60019, failed to inhibit mitophagy in either MCL or WT A-T cells (Figure 6A-C; *Online Supplementary Figure S7A, B*). As expected KU60019 inhibited FCCP-induced ATM^{Ser1981}, H2AX^{Ser139} and Kap1^{Ser824} phosphorylation in both MCL cell lines, but failed to rescue FCCP-induced loss of Tom20 and mitophagy (Figure 6D-F). Neither FCCP-induced Pink1 and Parkin activation, nor Parkin-UB^{Ser65} phosphorylation was inhibited by KU60019 (*Online Supplementary Figure S7C, D*). Furthermore, KU60019 could not inhibit CCCP-induced mitophagy in WT HeLa cells (Figure 6G, H).

Thirty-eight primary lymphomas, including MCL (n=21), marginal zone lymphoma (MZL, n=5), follicular lymphoma (FL, n=6) and diffuse large B-cell lymphoma (DLBCL, n=6), were analyzed (*Online Supplementary Table S2*) for their response to FCCP-induced mitophagy. B cells isolated from healthy donors (n=3) or peripheral blood mononuclear cells (n=2) served as controls. All samples were treated with IR and their ATM kinase status was determined by FCS analysis of PE-phospho-ATM^{Ser1981} and FITC-γH2AX^{Ser139} co-staining, while their mitophagy status was determined by FCS and immunoblot analyses (Figure 6I-K, P; *Online Supplementary Figures S8A-E, S9A, D* and *S10A-H*). Among all B-cell lymphomas screened, 13 (34%) were negative for IR-induced phospho-ATM^{Ser1981} and γH2AX^{Ser139} activation (IR$^-$) (MCL=8; FL=2; DLBCL=3). Among MCL subtypes, 13 lymphomas were positive for IR-induced phospho-ATM^{Ser1981} and γH2AX^{Ser139} activation (IR$^+$) and eight were IR$^-$; no statistical correlation was observed between IR$^+$ or IR$^-$ subtypes and their mitophagy status (Table 1; Figure 6K). Similarly, among all non-MCL subjects, no statistical correlation was observed between mitophagy, basal mROS and their ATM kinase status (Figure 6M; *Online Supplementary Figure S9A*). A higher abundance of mtDNA copy number was seen in all IR$^-$ MCL and non-MCL lymphomas (Figure 6L; *Online Supplementary Figure S9B*). Consistent with cell line data, FCCP-induced loss of $\Delta\Psi_m$ was prevalent in all primary

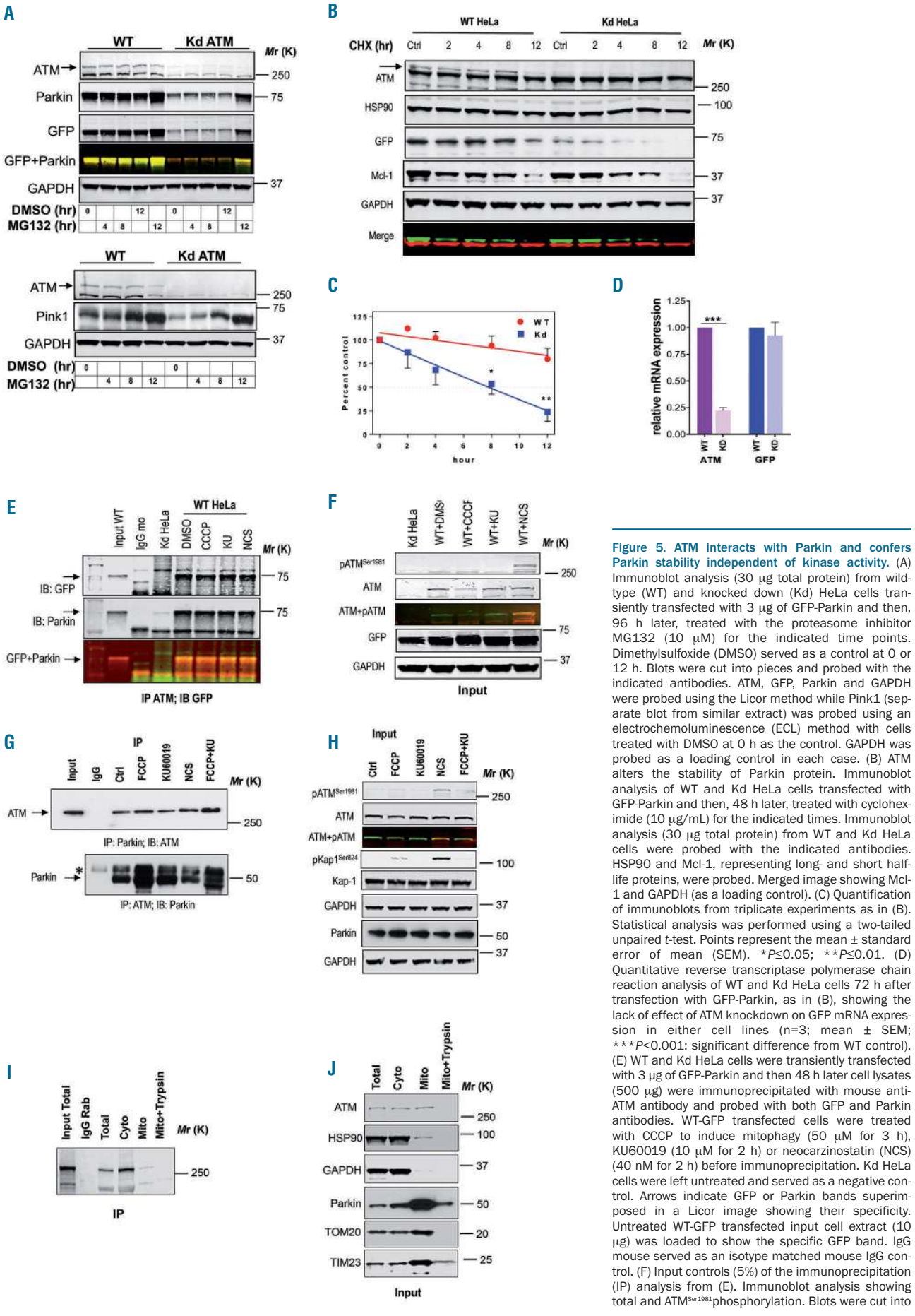

Figure 5. ATM interacts with Parkin and confers Parkin stability independent of kinase activity. (A) Immunoblot analysis (30 μg total protein) from wild-type (WT) and knocked down (Kd) HeLa cells transiently transfected with 3 μg of GFP-Parkin and then, 96 h later, treated with the proteasome inhibitor MG132 (10 μM) for the indicated time points. Dimethylsulfoxide (DMSO) served as a control at 0 or 12 h. Blots were cut into pieces and probed with the indicated antibodies. ATM, GFP, Parkin and GAPDH were probed using the Licor method while Pink1 (separate blot from similar extract) was probed using an electrochemoluminescence (ECL) method with cells treated with DMSO at 0 h as the control. GAPDH was probed as a loading control in each case. (B) ATM alters the stability of Parkin protein. Immunoblot analysis of WT and Kd HeLa cells transfected with GFP-Parkin and then, 48 h later, treated with cycloheximide (10 μg/mL) for the indicated times. Immunoblot analysis (30 μg total protein) from WT and Kd HeLa cells were probed with the indicated antibodies. HSP90 and Mcl-1, representing long- and short half-life proteins, were probed. Merged image showing Mcl-1 and GAPDH (as a loading control). (C) Quantification of immunoblots from triplicate experiments as in (B). Statistical analysis was performed using a two-tailed unpaired *t*-test. Points represent the mean ± standard error of mean (SEM). **P*≤0.05; ***P*≤0.01. (D) Quantitative reverse transcriptase polymerase chain reaction analysis of WT and Kd HeLa cells 72 h after transfection with GFP-Parkin, as in (B), showing the lack of effect of ATM knockdown on GFP mRNA expression in either cell lines (n=3; mean ± SEM; ****P*<0.001: significant difference from WT control). (E) WT and Kd HeLa cells were transiently transfected with 3 μg of GFP-Parkin and then 48 h later cell lysates (500 μg) were immunoprecipitated with mouse anti-ATM antibody and probed with both GFP and Parkin antibodies. WT-GFP transfected cells were treated with CCCP to induce mitophagy (50 μM for 3 h), KU60019 (10 μM for 2 h) or neocarzinostatin (NCS) (40 nM for 2 h) before immunoprecipitation. Kd HeLa cells were left untreated and served as a negative control. Arrows indicate GFP or Parkin bands superimposed in a Licor image showing their specificity. Untreated WT-GFP transfected input cell extract (10 μg) was loaded to show the specific GFP band. IgG mouse served as an isotype matched mouse IgG control. (F) Input controls (5%) of the immunoprecipitation (IP) analysis from (E). Immunoblot analysis showing total and ATM^{Ser1981}phosphorylation. Blots were cut into

pieces and probed with the indicated antibodies. GAPDH served as a loading control. (G) Endogenous co-immunoprecipitation of the Mino MCL cell line (500 μg for each treatment) either with rabbit anti-Parkin antibody and probed with mouse anti-ATM (upper lanes) or with rabbit anti-ATM antibody and probed with mouse anti-Parkin antibody (lower lanes, both ECL blots). Cells were pretreated with FCCP (50 μM for 3 h), KU60019 (10 μM for 1 h) or NCS (40 nM for 1 h) before IP. (H) Input controls (5%) of the IP analysis from Figure 5G. Immunoblot analysis showing FCCP-induced ATM^{Ser1981} phosphorylation or inhibition by KU60019. NCS served as a positive control for both ATM^{Ser1981} and Kap1^{Ser824} phosphorylation. Total and phosphorylated bands were merged and are shown in color for specificity. The Parkin blot was probed using ECL reagents. GAPDH was used as a loading control each time. (I) IP analysis of an endogenous ATM-Parkin interaction in total, cytoplasm, mitochondria or trypsin-digested mitochondria in untreated Mino cells (10x10^6 cells in each group) following cell fractionation. The Parkin-ATM interaction was detected in total, cytoplasm or in the untreated mitochondria but not in isolated mitochondria treated with trypsin. Isolated cellular fractions were immunoprecipitated with rabbit-Parkin antibody and probed with mouse ATM antibody. A 10 μL input control from the total cell extract was loaded to specify the ATM band. Rabbit IgG served as a negative control. (J) Input controls (5%) of the IP analysis from (I). Immunoblot analysis showing presence of ATM in total, cytoplasm, or in undigested mitochondria but not in isolated mitochondria treated with trypsin. GAPDH and HSP90 served as positive controls for their cytoplasmic abundance. Tom20 served as an outer mitochondrial membrane translocase while TIM23 represents an inner membrane translocase in trypsin-digested mitochondria.

MCL screened regardless of their IR status (Figure 6N; *Online Supplementary Figure S9D*). Cytogenetic analysis revealed that 18 subjects with MCL harbored the t(11;14) translocation and this was also unrelated to mitophagy (Figure 6O; Table 1; *Online Supplementary Table S2*). Immunoblot analysis established a strong correlation between IR-induced ATM^{Ser1981}, Kap1^{Ser824} and Smc1^{Ser966} phosphorylation, consistent with FCS analysis among all primary MCL and non-MCL lymphomas (Figure 6P; *Online Supplementary Figure S10A-H*).

Total and phospho ATM^{Ser1981} protein levels were either low or undetectable in the majority of subjects with MCL compared to the levels in MCL cell lines (Jeko-1 and Mino). Both Parkin and phospho-UB^{Ser65} Parkin levels were either low or undetectable in a subset of MCL subjects (MCL 2, 8, 15, 17, 19) (Figure 6P; *Online Supplementary Figure S10A-D*); IR-induced ATM^{Ser1981}, Kap1^{Ser824} and Smc1^{Ser966} phosphorylation was not detected in these lymphomas which were resistant to mitophagy. Similarly despite a lack of IR-induced ATM kinase activation, a subset of primary MCL activated phospho-Parkin-UB^{Ser65}-induced mitophagy (MCL 2, 4, 5) (Figure 6P). Conversely, analysis of basal Parkin protein expression in all primary lymphomas revealed a positive trend of higher Parkin expression among IR$^+$ lymphomas than among IR$^-$ lymphomas (Figure 6Q). These data further suggest that ATM kinase activity is not required *per se* for phospho-UB^{Ser65} activation-induced mitophagy in cells derived from patients.

Pink1 expression was either low or undetectable in a subset of MCL (MCL 2, 4, 8, 17, 19) (Figure 6P; *Online Supplementary Figures S8B* and *S10A-D*) and a few of these lymphomas (MCL 8, 17, 19) could not activate phospho-UB^{Ser65} Parkin and were resistant to mitophagy. Interestingly, mitophagy was not activated in a subset of IR$^+$ MCL (MCL 8, 13, 14, 19, 21) (*Online Supplementary Figures S8B* and *S10A-D*) suggesting a heterogeneous response. Inducible mitophagy was also prevalent among non-MCL lymphomas (*Online Supplementary Figures S9A* and *S10E-H*). Despite detectable ATM expression, IR could not activate ATM^{Ser1981}, Kap1^{Ser824} and Smc1^{Ser966} phosphorylation in a subset of DLBCL and FL (IR$^-$) while all MZL lymphomas were IR$^+$ (*Online Supplementary Figure S8C-E*). Consistent with MCL, a few IR$^+$ lymphomas (DLBCL4, DLBCL5, LBCL, SMZL1, FL1 and FL4) were resistant to mitophagy (*Online Supplementary Figure S9A; Supplementary Table S3*) while a few of the IR$^-$ lymphomas (DLBCL 1, 2 and FL 6) were mitophagy-proficient. No statistical correlation was observed between IR status, mROS or loss of $\Delta\Psi_m$ in these lymphomas, while mtDNA copy number (*Online Supplementary Figure S9B-D*) was higher in IR$^-$ FL and DLBCL. Although the majority of these lymphomas expressed Pink1 and Parkin, FCCP-induced phospho-UB^{Ser65} Parkin activation was not detected in a few lymphomas (DLBCL 4, 5 and FL 2) rendering them resistant to mitophagy.

Discussion

Mitophagy is a selective process of macro-autophagy eliminating intracellular pathogens and dysfunctional mitochondria by engulfing cargo into autophagolysomes[37] thereby maintaining mitochondrial homeostasis, genomic stability, and integrity of cells with other healthy organelles. Therefore, imposing an opportunistic and timely exclusion of dysfunctional mitochondria *via* mitophagy would be useful to protect cellular and genome integrity.

ATM^{Ser1981}autophosphorylation is considered a hallmark of ATM activation[38] and is important in maintaining genomic integrity.[39] Recent observations suggest that ATM plays an important role in mitophagy in both murine thymocytes as well as in A-T cells[23] but the mechanism is poorly understood. Parkin, a protein linked to Parkinson disease, is activated during mitophagy.[40,41] These key observations raise important questions regarding a possible link between Parkin and ATM. Parkin is a tumor-suppressor protein and is known to regulate cell cycle proteins including Cyclin D1, Cyclin E, and CDK4 in cancers,[42] while ATM is frequently lost and mutated in cancer thereby underscoring the need to evaluate their roles in mitophagy.

To explore the mechanism of ATM-dependent mitophagy in cancer, we selected MCL as a model system since ATM is the second most common alteration in MCL (>50%), in which ATM is frequently lost either by 11q deletion or mutation in the kinase domain and is associated with a high number of chromosomal alterations.[43] MCL is an aggressive form of non-Hodgkin lymphoma, and remains largely incurable; most affected patients eventually die of relapsed/refractory disease,[44] thereby arguing for a need for an alternative method of treatment.

We present evidence that cancer cell mitophagy is dependent on ATM but not its kinase activity and connects Parkin in this pathway. We show that ATM is required for mitophagy but not global autophagy. Furthermore we demonstrate that ATM, but not its kinase activity, is required for ionophore-induced dissipation of $\Delta\Psi_m$, a prerequisite signal required for Pink1-Parkin-mediated mitophagy.[45] Our data are in agreement with the notion that Pink1 activation leading to Parkin activation *via* UB^{Ser65} phosphorylation during mitophagy is in part ATM-dependent. We provide evidence that KU60019 failed to inhibit FCCP-induced Parkin-UB^{Ser65} phosphorylation and mitophagy in multiple cell lines. Based on these

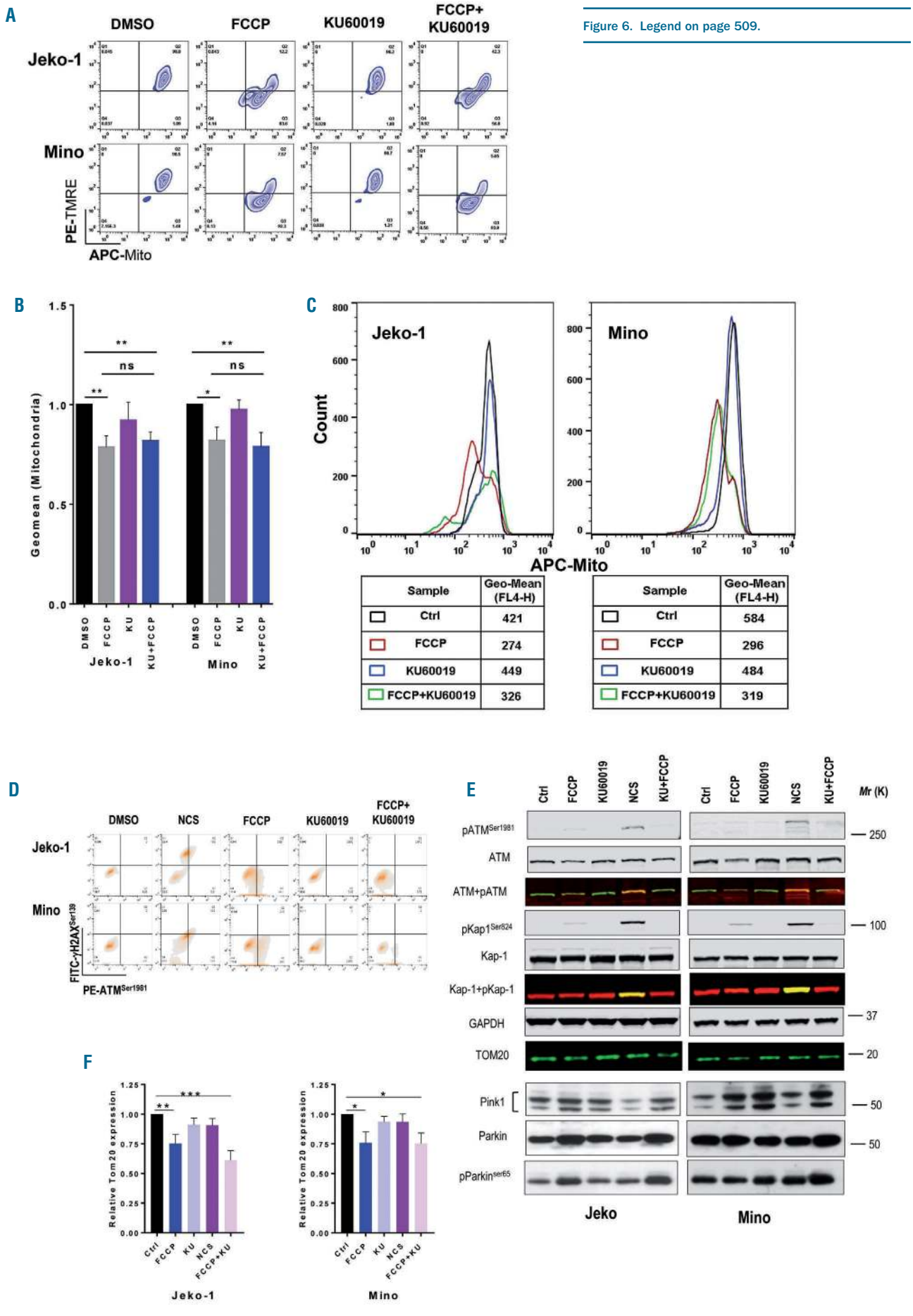

Figure 6. Legend on page 509.

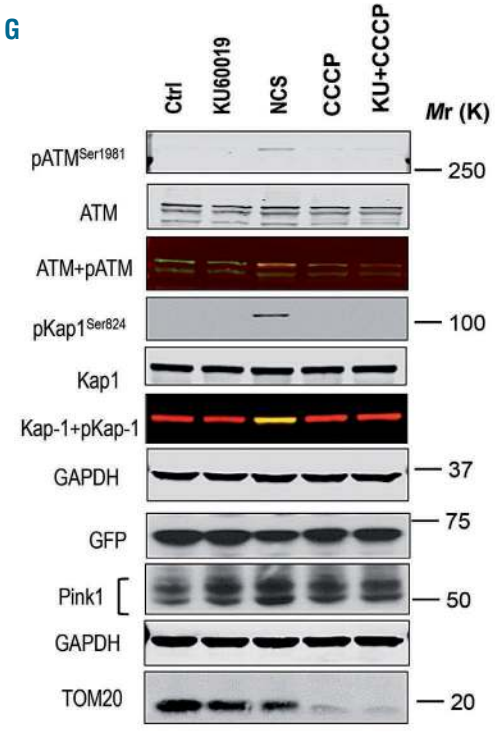

Figure 6. (continued) Legend on page 509.

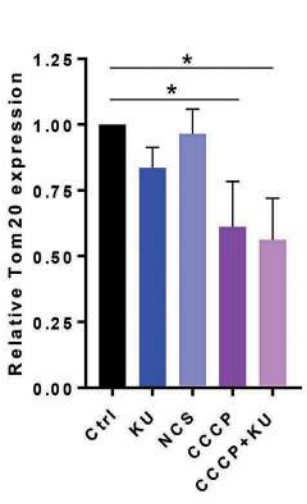

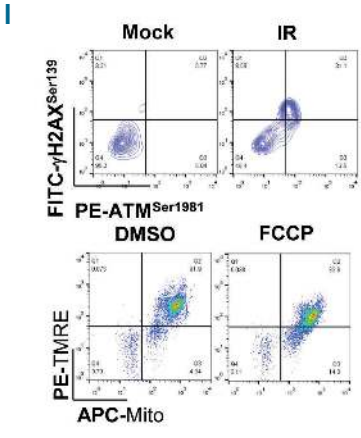

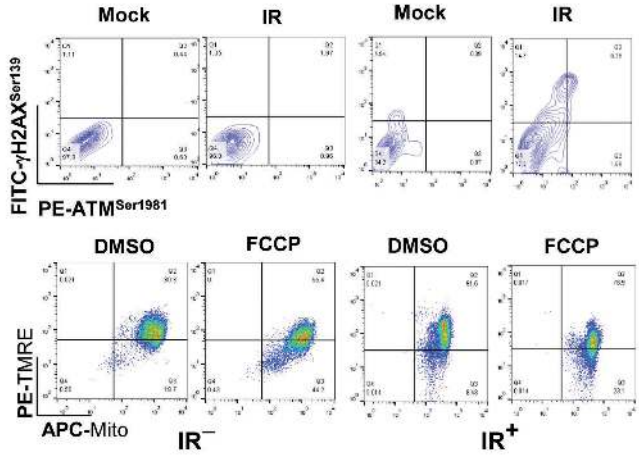

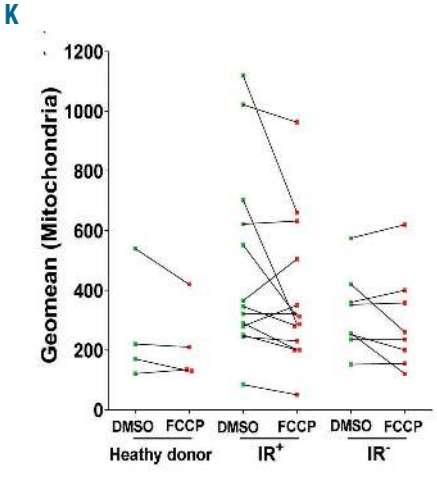

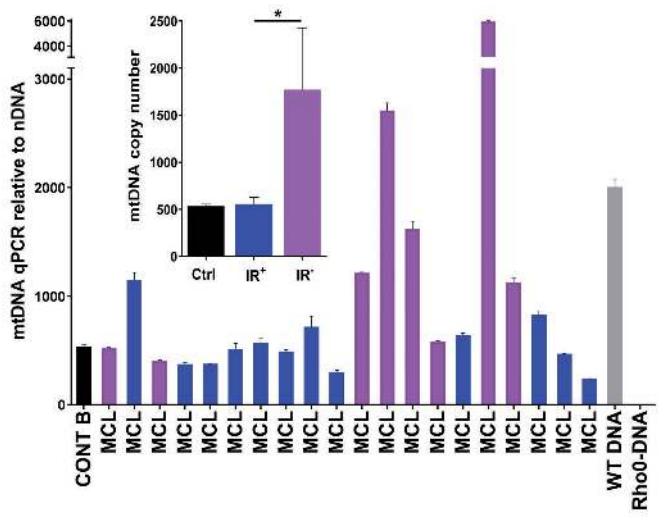

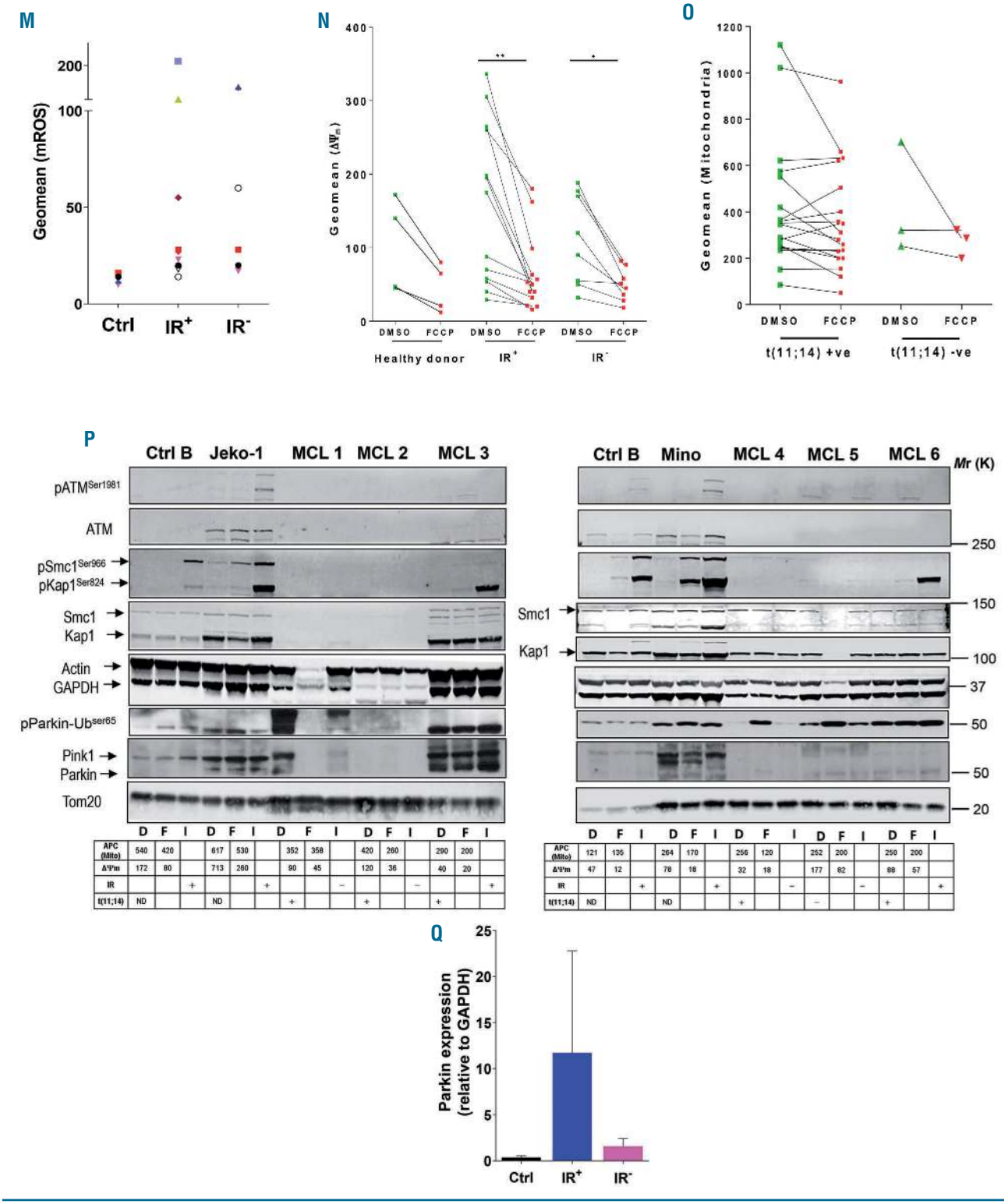

Figure 6. (continued) ATM kinase activity is dispensable in mitophagy in HeLa, mantle cell lymphoma cell lines and primary B-cell lymphomas. (A) Representative flow cytometry (FCS) data showing mitophagy in mantle cell lymphoma (MCL) cell lines ($5x10^6$ live cells) treated with FCCP (75 μM for 3 h) or the ATM kinase inhibitor, KU60019 (10 μM for 1 h), either alone or in combination. Following treatments, cells were washed and stained with TMRE (PE) and Mitotracker deep red (APC) and acquired by a FACSCalibur and analyzed with FlowJo software. (B) Relative geometric mean of mitochondrial mass, as in (A), in MCL cell lines treated with FCCP, KU60019 or their combination (mean ± standard error of mean [SEM]; n=7; *P<0.05, **P<0.01: significant difference from respective dimethylsulfoxide [DMSO] or FCCP controls). (C) Representative FCS profile of mitochondrial retention in MCL cell lines treated with FCCP, KU60019 or both in combination, as in (A). (D) FCS analysis showing inhibition of ATM phosphorylation by KU60019 in MCL cell lines, as in (A). Cells treated with neocarzinostatin (NCS) (40 nM for 1 h) served as a positive control. Following treatments, cells were stained with PE-ATM^{Ser1981} and FITC-γH2AX^{Ser139} (as in Figure 2B) and acquired by a FACSCalibur and analyzed with FlowJo software. (E) Immunoblot analysis (30 μg total protein) of MCL cell lines treated with FCCP, KU60019 or their combination, as in (A), and probed with the indicated antibodies. NCS treatment served as a positive control for both ATM^{Ser1981} and Kap1^{Ser824} activation. Total and phosphorylated bands were merged and are shown in color for specificity. Separate blots were cut into pieces and probed with the indicated antibodies. The levels of Parkin, phospho-UB^{Ser65} Parkin and Pink1 protein expression were detected by electrochemoluminescence (ECL). GAPDH was probed as a loading control each time. (F) Densitometry analysis of mitophagy (Tom20 expression) in MCL cell lines treated with the indicated compounds. Assays with FCCP, KU60019 or both in combination (n=7 in Jeko-1 or n=5 in Mino cells) and

NCS (n=5 in Jeko-1 and n=3 in Mino) were done. Data represent the mean ± SEM; *P<0.05, **P<0.01, ***P<0.001: significant differences from respective controls. (G) Immunoblot analysis (30 µg total protein) of WT HeLa cells treated with FCCP, KU60019 or their combination, as in (E), and probed with the indicated antibodies. NCS served as a positive control for both ATM^{Ser1981} and Kap1^{Ser824} activation. Total and phosphorylated bands were merged and are shown in color for specificity. Separate blots were cut into pieces and probed with the indicated antibodies. The levels of Parkin, phospho-UB^{Ser65} Parkin and Pink1 protein expression were detected by ECL. GAPDH was probed as a loading control each time. (H) Densitometry analysis of mitophagy (Tom20 expression) in WT HeLa cells treated with the indicated compounds, as in (F). Assays with FCCP, KU60019 or both in combination (n=6) and NCS (n=4) were performed. Data represent the mean ± SEM; *P<0.05: significant difference from the respective control. (I) Representative FCS analysis of irradiation (IR)-induced (5 Gray as in Figure 1G) ATM^{Ser1981} and +H2AX^{Ser139} phosphorylation in B cells isolated from healthy donors (upper panel) or FCCP (75 µM for 3 h)-induced mitophagy (as in Figure 1A; lower panel). (J) Representative FCS analysis showing IR^{-} and IR^{+} primary MCL lymphomas proficient or deficient in FCCP-induced mitophagy, respectively. (K) Line graph representation of the geometric mean of FCS analysis of mitochondrial retention in samples from four healthy donors (purified B cells in 3 cases and peripheral blood mononuclear cells in 1 case) or from 21 patients with primary MCL showing their individual IR status (IR^{+} n=13; IR^{-} n=8) and their response to FCCP-induced mitophagy. (L) Quantitative polymerase chain reaction (qRT-PCR) analysis (as in Figure 2I) of mitochondrial DNA (mtDNA) copy number in 20 primary MCL (IR^{+} n=12 and IR^{-} n=8) or control healthy donor B cells (n=3). WT DNA and Rho0-DNA served as positive and negative controls for mtDNA qRT-PCR analysis. Inset showing mean ± SEM; *P<0.05 significant difference from IR^{+} lymphomas. (M) Relative geometric mean of basal mitochondrial reactive oxygen species (mROS) levels (as in Figure 1D) in healthy donor B cells (n=3) or primary MCL (IR^{+} n=9 and IR^{-} n=5). (N) Line graph representation of the geometric mean of FCS analysis of mitochondrial membrane potential ($\Delta\Psi_m$) following FCCP treatment of cells from four healthy donors (3 purified B cells in 3 cases and peripheral blood mononuclear cells in 1 case) and from 21 patients with primary MCL showing their IR status (IR^{+} n=13; IR^{-} n=8) and their response to FCCP-induced loss of $\Delta\Psi_m$. *P<0.05, **P<0.01: significant differences from respective DMSO controls. (O) FCS analysis showing geometric means of mitochondrial mass following FCCP-induced mitophagy in cells from 21 patients with primary MCL and their respective t(11;14) status (positive n=18; negative n=3). (P) Immunoblot analysis showing FCCP-induced mitophagy in control B cells, MCL cell lines or six primary MCL cases (30 µg total protein), probed with the indicated antibodies. Corresponding IR- or FCCP-induced FCS analysis data are shown in the tables underneath. The levels of Parkin, phospho-UB^{Ser65} Parkin and Pink1 protein expression were determined by an ECL method. Both actin and GAPDH were probed as loading controls. D: DMSO; F: FCCP; I: IR. (Q) Densitometry analysis of Parkin expression in purified B cells from healthy donors (n=3) or IR^{+} (n=22) and IR^{-} (n=8) lymphomas (including MCL, marginal zone lymphoma, diffuse large B-cell lymphoma and follicular lymphoma). Data represent mean ± SEM.

observations, we propose that ATM kinase activity is dispensable for Parkin activation. Moreover, we observed that mitophagy inhibition following loss of ATM promotes high mROS and mtDNA copy number, low mitochondrial respiration, and ATP generation. However, none of these phenotypes clearly explains the role of ATM kinase in mitophagy.

The loss of stable GFP-Parkin levels in ATM-deficient HeLa cells suggests a novel link between ATM and mitophagy *via* kinase-independent, ATM-Parkin physical interactions. In normal basal condition cytosolic Parkin exists in a coiled and auto-inhibited 'closed' conformation and in an inactive state.[46-48] Conversely Parkin ubiquitinates itself and promotes its own degradation and we demonstrated that MG132 rescued GFP-Parkin degradation in shATM HeLa cells. Consistent with this observation, we also showed ablation of ATM in MCL cell lines triggers loss of endogenous Parkin expression. These observations support the notion that ATM may play a role in conferring Parkin stability and thereby contribute to mitophagy. However, this phenomenon is in contrast to the situation in A-T cells in which Parkin is expressed in the absence of ATM, suggesting a context-specific interaction. The stability of Parkin in tumor and non-tumor cells may enforce different mechanisms. This apparent discrepancy could be due to the possibility that non-tumor A-T fibroblasts utilize an ATM-independent mechanism to stabilize Parkin.

Regardless, we show that ATM kinase activity is dispensable for the ATM-Parkin interaction. Both KU60019 and kinase-dead ATM (KD-ATM) complex with Parkin (or GFP-Parkin) in multiple cancer cell lines. This novel ATM-kinase-independent affinity to complex with Parkin was further supported by the observation that ATM protein but not its kinase activity is required for mitophagy. Our data are in contrast with those of spermidine-induced mitophagy through ATM kinase-dependent activation of the PINK1/Parkin pathway in A-T fibroblasts.[49] Moreover, recent studies provide evidence of the presence of mitochondrial Parkin[23] in untreated A-T fibroblasts suggesting that ATM may not be required for mitochondrial Parkin translocation. However, we show that FCCP triggered both PINK1 and Parkin accumulation, consistent with spermidine-induced mitophagy.[49] A recent study demonstrated that KU60019 treatment alleviates senescence *via* restoration, functional recovery and re-acidification of the lysosome/autophagy system and metabolic reprogramming.[50] Therefore, ATM kinase negatively regulates terminal mitochondrial destruction *via* strict control of lysosomal pH, underscoring our observation.

Our data also contradict the role of ATM kinase in mitophagy in multiple cancer cell lines and in primary lymphomas. Consistent with data from shATM cell lines and given that upstream Pink1 kinase activates and recruits Parkin into depolarized mitochondria, we also present evidence that ATM kinase activity is not required for either Parkin-UB^{Ser65} phosphorylation or upstream Pink1 activation since neither inhibition of ATM kinase by KU60019 nor activation of kinase activity by neocarzinostatin affected the ATM-Parkin interaction or Parkin-UB^{Ser65} phosphorylation. Similarly, despite heterogeneity among primary B-cell lymphomas, we did not see evidence of ATM kinase dependency in mitophagy. Consistent with the cell line data, we showed that ATM is not required for loss of $\Delta\Psi_m$, and mitophagy is not controlled by the MCL-specific t(11;14) translocation in primary lymphomas. Although we do not know the 11q status of these lymphomas, a few primary MCL do not express detectable ATM in immunoblots and also have low or undetectable Parkin expression. Based on our IR-induced kinase screening assay, we predict several lymphomas may have lost ATM protein and a subset of these lymphomas lack either Pink1 or Parkin proteins. Moreover, a few ATM kinase deficient (IR^{-}) lymphomas also activated FCCP-induced Parkin-UB^{Ser65} phosphorylation suggesting that ATM kinase activity is dispensable for Parkin activation. It is likely that while Parkin (PARK2) is frequently deleted in human cancers and associated with CCND1 overexpression[42] may also contribute to cell proliferation in MCL and confers resistance to mitophagy.

In conclusion, loss of ATM protein may not only contribute to genotoxic stress through ROS production but can also provoke adverse effects including loss of Parkin, preservation of defective mitochondria, inhibition of mitophagy and low mitochondrial respiration, all of which may contribute to refractory diseases. We propose a pathway in which ATM but not its kinase activity is associated with induction of mitophagy through an ATM-Parkin interaction in cancer cells underscoring the

Table 1. Flow cytometry analysis of the response of primary mantle cell lymphoma to FCCP-induced mitophagy is independent of ATM kinase activity.

			Mitophagy Status		$\Delta\psi_m$ Status			
	t(11;14) status	IR status	DMSO	FCCP	DMSO	FCCP	mROS	mtDNA copy number
1	t(11;14)	-	352	358	90	45	20	524
2	t(11;14)	-	420	260	120	36	17	580
3	t(11;14)	+	290	200	40	20	20	718
4	t(11;14)	-	256	120	32	18	28	1621
5		-	252	200	177	82	ND	405
6	t(11;14)	+	250	200	88	57	ND	489
7	t(11;14)	-	152	155	55	51	153	5970
8		+	321	322	58	32	28	377
9	t(11;14)	+	244	230	260	180	20	297
10		+	703	287	54	16	23	830
11	t(11;14)	+	346	280	175	50	27	640
12	t(11;14)	-	235	235	170	77	ND	2711
13	t(11;14)	+	280	350	195	40	ND	236
14	t(11;14)	+	365	505	336	99	ND	573
15	t(11;14)	+	84	50	29	21	14	468
16	t(11;14)	+	552	312	265	40	210	512
17	t(11;14)	-	575	620	188	58	60	1215
18	t(11;14)	-	360	400	50	28	150	1141
19	t(11;14)	+	622	632	198	63	125	1151
20	t(11;14)	+	1120	660	70	53	18	372
21	t(11;14)	+	1022	963	305	162	55	ND

Live cells ($5x10^6$) were irradiated (5 Gray, as in Figure 1G). Cells were stained with PE-ATM^{Ser1981} and FITC-γH2AX^{Ser139} to determine their ATM kinase status (*Online Supplementary Figure S8*) or treated with FCCP (75 μM for 3 h) and stained with PE-TMRE to determine mitochondrial membrane potential ($\Delta\Psi_m$), or APC-Mitotracker deep red to determine mitochondria mass and deduce their mitophagy response. Untreated cells were stained with MitoSOX Red to determine the basal level of mitochondrial reactive oxygen species. Mitochondrial DNA copy number was analyzed from total cellular DNA isolated from untreated cells by quantitative polymerase chain reaction analysis (see Methods). ND: not determined.

first described molecular role of ATM in mitochondrial autophagy. Pharmacological targeting of mitophagy through ATM and Parkin, in combination with other drugs or stresses, may offer opportunities to control tumor progression because of the acute sensitivity of tumor cells to mitochondrial dysfunction.

Disclosures

No conflicts of interests to disclose.

Contributions

A.S. conceptualized the study, designed experiments, generated and analyzed data, and wrote the manuscript. CMS contributed and provided critical reagents related to autophagy studies and was involved in designing and analyzing the protein half-life and mRNA qPCR studies. HVV contributed in Seahorse XF96 Analyzer and in OCR studies. M.A. performed NTP assays and HPLC analysis. B.A.K. and J.P contributed in qPCR analysis of mtDNA experiments. KB and A.S. contributed in FCS assays related to cytotoxicity. JKB and WNH contributed in confocal analyses. TKP contributed critical reagents and technical help related to ATM kinase function. SSN identified patients and provided primary B-cell lymphoma cells and their cytogenetic characteristics. VG supervised the research project, analyzed data, obtained funding, and reviewed the manuscript. TKP, WNH, CMS and VG contributed in writing/editing the manuscript.

Acknowledgments

We thank Dr. Sankar Mitra, Methodist Research Institute, Houston, TX, USA for crtically reviewing the manuscript. We also thank Dr. Richard Youle, NIH for providing us with the YFP-Parkin plasmid, Dr. Noriyuki Matsuda, Tokyo Metropolitan Institute of Medical Science, Tokyo, Japan for providing us with the GFP-Parkin construct and Rakesh Sharma, Department of Lymphoma/Myeloma, MD Anderson Cancer Center, Houston, TX, USA for processing and distributing the primary B-cell lymphomas. This work was supported by a CLL Global Research Foundation Alliance grant. A part of this work was performed in the Flow Cytometry and Cellular Imaging Facility, supported in part by the NIH through MD Anderson's Cancer Center Support grant CA016672.

References

1. Brandon M, Baldi P, Wallace DC. Mitochondrial mutations in cancer. Oncogene. 2006;25(34):4647-4662.
2. Fulda S, Galluzzi L, Kroemer G. Targeting mitochondria for cancer therapy. Nat Rev Drug Discov. 2010;9(6):447-464.
3. Galluzzi L, Joza N, Tasdemir E, et al. No death without life: vital functions of apoptotic effectors. Cell Death Differ. 200815(7): 1113-1123.
4. Sabharwal SS, Schumacker PT. Mitochondrial ROS in cancer: initiators, amplifiers or an Achilles' heel? Nature Rev Cancer. 2014;14(11):709-721.
5. Vander Heiden MG, Cantley LC, et al. Understanding the Warburg effect: the metabolic requirements of cell proliferation. Science. 2009;324(5930):1029-1033.

6. Van Houten B, Woshner V, Santos JH. Role of mitochondrial DNA in toxic responses to oxidative stress. DNA Repair (Amst). 2006;5(2):145-152.
7. de Moura MB, dos Santos LS, Van Houten B. Mitochondrial dysfunction in neurodegenerative diseases and cancer. Environ Mol Mutagen. 2010;51(5):391-405.
8. Diehn M, Cho RW, Lobo NA, et al. Association of reactive oxygen species levels and radioresistance in cancer stem cells. Nature. 2009;458(7239):780-783.
9. Kroemer G, Pouyssegur J. Tumor cell metabolism: cancer's Achilles' heel. Cancer Cell. 2008;13(6):472-482.
10. Liesa M, Palacin M, Zorzano A. Mitochondrial dynamics in mammalian health and disease. Physiol Rev. 2009;89(3):799-845.
11. Westermann B. Mitochondrial fusion and fission in cell life and death. Nat Rev Mol Cell Biol. 2010;11(12):872-884.
12. Youle RJ, van der Bliek AM. Mitochondrial fission, fusion, and stress. Science. 2012;337(6098):1062-1065.
13. Narendra DP, Jin SM, Tanaka A, et al. PINK1 is selectively stabilized on impaired mitochondria to activate Parkin. PLoS Biol. 2010;8(1):e1000298.
14. Youle RJ, Narendra DP. Mechanisms of mitophagy. Nat Rev Mol Cell Biol. 2011;12(1):9-14.
15. Pickrell AM, Youle RJ. The roles of PINK1, parkin, and mitochondrial fidelity in Parkinson's disease. Neuron. 2015;85(2):257-273.
16. Ditch S, Paull TT. The ATM protein kinase and cellular redox signaling: beyond the DNA damage response. Trends Biochem Sci. 2012;37(1):15-22.
17. Lavin MF, Shiloh Y. Ataxia-telangiectasia: a multifaceted genetic disorder associated with defective signal transduction. Curr Opin Immunol. 1996;8(4):459-464.
18. Udayakumar D, Horikoshi N, Mishra L, et al. Detecting ATM-dependent chromatin modification in DNA damage response. Methods Mol Biol. 2015;1288:317-336.
19. Shiloh Y. ATM and related protein kinases: safeguarding genome integrity. Nature Rev Cancer. 2003;3(3):155-168.
20. You Z, Shi LZ, Zhu Q, et al. CtIP links DNA double-strand break sensing to resection. Mol Cell. 2009;36(6):954-969.
21. Barlow C, Ribaut-Barassin C, Zwingman TA, et al. ATM is a cytoplasmic protein in mouse brain required to prevent lysosomal accumulation. Proc Natl Acad Sci U S A. 2000;97(2):871-876.
22. Lim DS, Kirsch DG, Canman CE, et al. ATM binds to beta-adaptin in cytoplasmic vesicles. Proc Natl Acad Sci U S A. 1998;95(17):10146-10151.
23. Valentin-Vega YA, Maclean KH, Tait-Mulder J, et al. Mitochondrial dysfunction in ataxia-telangiectasia. Blood. 2012;119(6):1490-1500.
24. Eaton JS, Lin ZP, Sartorelli AC, et al. Ataxia-telangiectasia mutated kinase regulates ribonucleotide reductase and mitochondrial homeostasis. J Clin Invest. 2007;117(9):2723-2734.
25. Ambrose M, Goldstine JV, Gatti RA. Intrinsic mitochondrial dysfunction in ATM-deficient lymphoblastoid cells. Hum Mol Genet. 2007;16(18):2154-2164.
26. Schaffner C, Idler I, Stilgenbauer S, et al. Mantle cell lymphoma is characterized by inactivation of the ATM gene. Proc Natl Acad Sci U S A. 2000;97(6):2773-2778.
27. Fang NY, Greiner TC, Weisenburger DD, et al. Oligonucleotide microarrays demonstrate the highest frequency of ATM mutations in the mantle cell subtype of lymphoma. Proc Natl Acad Sci U S A. 2003;100(9):5372-5377.
28. Venegas V, Halberg MC. Measurement of mitochondrial DNA copy number. Methods Mol Biol. 2012;837:327-335.
29. Amin HM, McDonnell TJ, Medeiros LJ, et al. Characterization of 4 mantle cell lymphoma cell lines. Arch Pathol Lab Med. 2003;127(4):424-431.
30. Vorechovsky I, Luo L, Dyer MJ, et al. Clustering of missense mutations in the ataxia-telangiectasia gene in a sporadic T-cell leukaemia. Nat Genet. 1997;17(1):96-99.
31. Salaverria I, Perez-Galan P, Colomer D, et al. Mantle cell lymphoma: from pathology and molecular pathogenesis to new therapeutic perspectives. Haematologica. 2006;91(1):11-16.
32. Pawlyk AC, Giasson BI, Sampathu DM, et al. Novel monoclonal antibodies demonstrate biochemical variation of brain parkin with age. J Biol Chem. 2003;278(48):48120-48128.
33. Chaugule VK, Burchell L, Barber KR, et al. Autoregulation of Parkin activity through its ubiquitin-like domain. EMBO J. 2011;30(14):2853-2867.
34. Yamano K, Youle RJ. PINK1 is degraded through the N-end rule pathway. Autophagy. 2013;9(11):1758-1769.
35. Schwanhausser B, Busse D, Li N, et al. Global quantification of mammalian gene expression control. Nature. 2011;473(7347):337-342.
36. Donzeau M, Kaldi K, Adam A, et al. Tim23 links the inner and outer mitochondrial membranes. Cell. 2000;101(4):401-412.
37. Lazarou M, Sliter DA, Kane LA, et al. The ubiquitin kinase PINK1 recruits autophagy receptors to induce mitophagy. Nature. 2015;524(7565):309-314.
38. Bakkenist CJ, Kastan MB. DNA damage activates ATM through intermolecular autophosphorylation and dimer dissociation. Nature. 2003;421(6922):499-506.
39. Lee JH, Paull TT. Activation and regulation of ATM kinase activity in response to DNA double-strand breaks. Oncogene. 2007;26(56):7741-7748.
40. Hang L, Thundyil J, Lim KL. Mitochondrial dysfunction and Parkinson disease: a Parkin-AMPK alliance in neuroprotection. Ann N Y Acad Sci. 2015;1350: 37-47.
41. Kazlauskaite A, Muqit MM. PINK1 and Parkin - mitochondrial interplay between phosphorylation and ubiquitylation in Parkinson's disease. FEBS J. 2015;282(2):215-223.
42. Gong Y, Zack TI, Morris LG, et al. Pan-cancer genetic analysis identifies PARK2 as a master regulator of G1/S cyclins. Nat Genet. 2014;46(6):588-594.
43. Bea S, Valdes-Mas R, Navarro A, et al. Landscape of somatic mutations and clonal evolution in mantle cell lymphoma. Proc Natl Acad Sci U S A. 2013 ;110(45):18250-18255.
44. Campo E, Rule S. Mantle cell lymphoma: evolving management strategies. Blood. 2015;125(1):48-55.
45. Narendra D, Tanaka A, Suen DF, et al. Parkin is recruited selectively to impaired mitochondria and promotes their autophagy. J Cell Biol. 2008;183(5):795-803.
46. Riley BE, Lougheed JC, Callaway K, et al. Structure and function of Parkin E3 ubiquitin ligase reveals aspects of RING and HECT ligases. Nat Commun. 2013;4:1982-1997.
47. Wauer T, Komander D. Structure of the human Parkin ligase domain in an autoinhibited state. EMBO J. 2013;32(15):2099-2112.
48. Trempe JF, Sauve V, Grenier K, et al. Structure of parkin reveals mechanisms for ubiquitin ligase activation. Science. 2013;340(6139):1451-1455.
49. Qi Y, Qiu Q, Gu X, et al. ATM mediates spermidine-induced mitophagy via PINK1 and Parkin regulation in human fibroblasts. Sci Rep. 2016;6:24700.
50. Kang HT, Park JT, Choi K, et al. Chemical screening identifies ATM as a target for alleviating senescence. Nat Chem Biol. 2017;13(6):616-623.